เซลล์แสงอาทิตย์โครงสร้างเฮตเตอโรชนิดอะลูมิเนียมแกลเลียมอาร์เซนายด์/แกลเลียมอาร์เซนายด์

นาย บุญปอน แก้วมณีวงศ์

ศูนย์วิทยทรัพยากร
จุฬาลงกรณ์มหาวิทยาลัย

วิทยานิพนธ์นี้เป็นส่วนหนึ่งของการศึกษาตามหลักสูตรปริญญาวิศวกรรมศาสตรมหาบัณฑิต
สาขาวิชาวิศวกรรมไฟฟ้า ภาควิชาวิศวกรรมไฟฟ้า
คณะวิศวกรรมศาสตร์ จุฬาลงกรณ์มหาวิทยาลัย
ปีการศึกษา 2553

ลิขสิทธิ์ของจุฬาลงกรณ์มหาวิทยาลัย

AlGaAs/GaAs HETEROSTRUCTURE SOLAR CELLS

Mr. Bounpone Keomanivong

A Thesis Submitted in Partial Fulfillment of the Requirements

for the Degree of Master of Engineering Program in Electrical Engineering

Department of Electrical Engineering

Faculty of Engineering

Chulalongkorn University

Academic Year 2010

Copyright of Chulalongkorn University

ศูนย์วิทยทรัพยากร
จุฬาลงกรณ์มหาวิทยาลัย

Thesis Title	AlGaAs/GaAs HETEROSTRUCTURE SOLAR CELLS
By	Mr. Bounpone Keomanivong
Field of Study	Electrical Engineering
Thesis Advisor	Professor Somsak Panyakeow, Ph.D.
Thesis Co-Advisor	Associate Professor Choompol Antarasena, Dr.Ing.

Accepted by the Faculty of Engineering, Chulalongkorn University in Partial Fulfillment of the Requirements for the Master's Degree

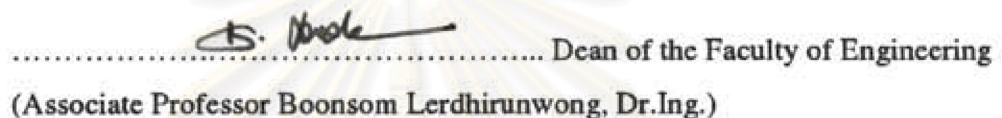
.... Dean of the Faculty of Engineering

(Associate Professor Boonsom Lerdhirunwong, Dr.Ing.)

THESIS COMMITTEE

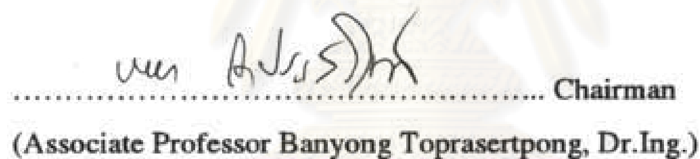
.... Chairman

(Associate Professor Banyong Toprasertpong, Dr.Ing.)

.... Thesis Advisor

(Professor Somsak Panyakeow, Ph.D.)

.... Thesis Co-Advisor

(Associate Professor Choompol Antarasena, Dr.Ing.)

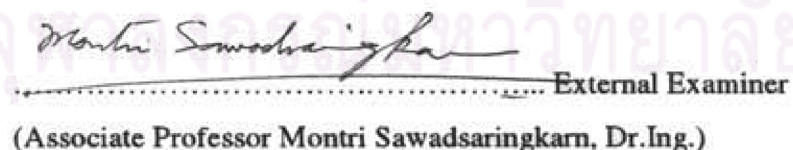
.... External Examiner

(Associate Professor Montri Sawadsaringkarn, Dr.Ing.)

ศูนย์วิทยทรัพยากร
จุฬาลงกรณ์มหาวิทยาลัย

บุญปอน แก้วมณีวงศ์: เซลล์แสงอาทิตย์โครงสร้างเฮตเตอโรชนิดอะลูมิเนียมแกลเลียมอาร์เซนายด์/แกลเลียมอาร์เซนายด์. (AlGaAs/GaAs HETEROSTRUCTURE SOLAR CELLS). อ.ที่ปรึกษาวิทยานิพนธ์หลัก: ศ.ดร.สมศักดิ์ ปัญญาแก้ว, อ.ที่ปรึกษาวิทยานิพนธ์ร่วม: รศ.ดร.ชุมพล อันตรเสน, 72 หน้า.

เซลล์แสงอาทิตย์โครงสร้างเฮตเตอโร จำนวน 8 โครงสร้าง ถูกออกแบบและทำการผลิตด้วยเทคโนโลยีปลูกผลึกชนิด MBE และชนิด LPE เซลล์แสงอาทิตย์กลุ่มแรก 6 โครงสร้าง ซึ่งประกอบด้วย ไดโอดแบบชอตกี้แบเรียของ *GaAlAs* จำนวน 1โครงสร้าง ไดโอดหัวต่อเฮตเตอโร GaAlAs(n)/GaAs(p) แบบมีชั้นหน้าต่างช่องว่างแถบพลังงานคงที่ จำนวน 1โครงสร้าง และ ไดโอดหัวต่อเฮตเตอโร GaAlAs(n)/GaAs(p) แบบมีชั้นหน้าต่างช่องว่างแถบพลังงานเป็นขั้นบันได จำนวน 4โครงสร้าง ถูกผลิตด้วย MBE ในขณะที่อีก 2 โครงสร้างของไดโอดหัวต่อเฮตเตอโร GaAlAs(P)/GaAs(n) แบบมีชั้นหน้าต่างช่องว่างแถบพลังงานคงที่ ผลิตด้วย LPE จากนั้นนำทุกตัวอย่างมาวัด ลักษณะสมบัติทางแสง และทางไฟฟ้า เห็นได้ชัดเจนว่าชั้นรับแสงช่องว่างแถบพลังงานกว้างของเซลล์แสงอาทิตย์โครงสร้างเฮตเตอโร แสดงความเป็นหน้าต่างแสงได้ชัดเจน แต่ชั้นหน้าต่างแสงก็ไม่สามารถช่วยปรับปรุงสมรรถนะของเซลล์แสงอาทิตย์ที่ผลิตได้ สรุปในภาพรวมเซลล์แสงอาทิตย์ทำงานที่ 1 ซัน แสดงค่า กระแสลัดวงจร (I_{sc}) อยู่ในช่วงระหว่าง 0.6 ถึง 1.5 มิลลิแอมป์ (mA), แรงดันวงจรเปิด (V_{oc}) อยู่ในช่วงระหว่าง 0.43 ถึง 0.7 โวลต์ (Volt) กำลังไฟฟ้าสูงสุด อยู่ในช่วงระหว่าง 0.15 ถึง 0.5 มิลลิวัตต์ (mW) ฟิลล์แฟกเตอร์ (FF) อยู่ในช่วงระหว่าง 0.38 ถึง 0.61 และ ประสิทธิภาพ (η) อยู่ในช่วงระหว่าง 2.3 ถึง 5 % สาเหตุหลักที่ทำให้เซลล์ทั้งหมดมีสมรรถนะต่ำ มาจากคุณภาพของผลึกและหัวต่อที่ไม่ดี รวมทั้งโครงสร้างที่ได้รับการออกแบบยังไม่เหมาะสม

ศูนย์วิทยทรัพยากร จุฬาลงกรณ์มหาวิทยาลัย

ภาควิชา วิศวกรรมไฟฟ้า................	ลายมือชื่อนิสิต..........................
สาขาวิชา วิศวกรรมไฟฟ้า...............	ลายมือชื่อ อ.ที่ปรึกษาวิทยานิพนธ์หลัก............
ปีการศึกษา 2553........................	ลายมือชื่อ อ.ที่ปรึกษาวิทยานิพนธ์ร่วม............

##5171632821: MAJOR ELECTRICAL ENGINEERING
KEYWORDS : AlGaAs, GaAs AND AlGaAs/GaAs HETERSTRUCTURE SOLAR CELL.

BOUNPONE KEOMANIVONG: AlGaAs/GaAs HETEROSTRUCTURE SOLAR CELLS. ADVISOR: PROF. SOMSAK PANYAKEOW, Ph.D., CO-ADVISOR: ASSOC. PROF. CHOOMPOL ANTARASENA, Dr.Ing. 72 pp.

Eight structures of Heterostructure Solar Cells have been designed and fabricated, by Molecular Beam Epitaxy (MBE) and by Liquid Phase Epitaxy (LPE) technologies. The first group, which consists of six structures: one of GaAlAs Schottky Barrier Diode, one of constant band gap window layer GaAlAs(p)/GaAs(n) heterojunction and three of step or stair case band gap window layer GaAlAs(n)/GaAs(p) heterojunction were realized by MBE, whereas the other two structures of constant band gap window layer GaAlAs(P)/GaAs(n) heterojunction were produced by LPE. Optical and electrical properties of all samples were then examined. It is evident that the GaAlAs wide band gap window layer of all heterostructure solar cells can behave in the role of window effect but it can not improve the overall performance of solar cells as expected. In conclusion, these solar cells perform at 1 sun with short circuit current (I_{sc}) in the range of 0.6 to $1.5\,mA$, open circuit voltage (V_{oc}) in the range of 0.43 to 0.7 Volt, maximum output power (P_{max}) in the range of 0.15 to 0.5 mW, fill factor (FF) in the range of 0.38 to 0.61 and efficiency (η) in the range of 2.3 to 5 %. The main reasons that cause all samples to have low performance are due to low quality of the crystal layers and of junction interface, together with unsuitable designed structures.

Department: ….. Electrical Engineering………….. Student's Signature ……….
Field of Study:...Electrical Engineering…………… Advisor's Signature ………..
Academic Year:..2010……………………………… Co-Advisor's Signature…………

ACKNOWLEDGEMENTS

I would like to firstly express my profound gratitude and appreciation to my kind advisor; Prof. Dr. Somsak Panyakeow, for his helpfulness and meaningful advices. He always shared his valuable time to cooperatively discuss my research. My deepest thankfulness is also addressed to my co-advisor; Assoc. Prof. Dr. Choompol Antarasena, for his friendly discussion, guidance, and supportive thought. In particular, working with them was an excellent chance for me to gain more invaluable knowledge and experiences which will be useful for the next step in my life.

My thanks and respects are also given to my thesis committees; Assoc. Prof. Dr. Banyong Toprasertpong and Assoc. Prof. Dr. Montri Sawadsaringkarn, who are friendly and generous lecturers. They kindly provided me fruitful suggestions and comments for conducting my research. Moreover, I would like to thank all lecturers in Chulalongkorn University, who gave me useful instructions and advices to expand my knowledge.

My profound thanks is given to all of Lecturers of Semiconductor Devices Research Laboratory (SDRL), who kindly help me to have a chance to do the experiment to get the necessary data and information for conducting my thesis. Unforgettably, I wish to deeply thank Mr. Supachok Thainoi, Mr. Pornchai Changmoang, Mr. Ongarj Tangmattajittakul, Mr. Chalernchai Himwas, and Mr. Nirat Patanasemakul for their continuous help and strong cooperation in my experiment at SDRL.

I would like to extend my grateful thanks to all official staffs employed in International School of Engineering and AUN/SEED-Net, who always distributed the updated information to me. I also thank to AUN/SEED-Net which was the main financial supporter for me.

Finally, very special thank from the bottom of my heart is gratefully addressed to my respectful parents; Kee Keomanivong and Chanh Keomanivong, and my beloved sister, who constantly cared and encouraged me every time I felt down. My parents have tried to do everything and worked hard all the time in order to enable their son and daughter to be able to study from primary school until university. One thought is given to them “I am very proud to be your son”.

CONTENTS

ABSTRACT (THAI)……………………………………………………………iv
ABSTRACT (ENGLISH)…………………………………………………………..v
ACKNOWLEDGEMENTS…………………………………………………….vi
CONTENTS……………………………………………………………………vii
LIST OF FIGURES…………………………………………………………...ix
LIST OF TABLES…………………………………………………………...xii

CHAPTER I: INTRODUCTION…………………………………………………1
1.1 Introduction……………………………………………………………1
1.2 Problem statements……………………………………………………4
1.3 Objective………………………………………………………………4
1.4 Scope of research……………………………………..……….……4
1.5 Research methodology………………………………………………4
1.6 Expected benefits……………………………………………………5

CHAPTER II: FUNDAMENTAL OF SOLAR CELL……………………………...6
2.1 General…………………………………………………………………6
2.2 Fundamental definition, and operation of solar cells………………………..6
2.2.1 Spectral response and collection efficiency……………………………8
2.3 Output characteristics of solar cells……………………………………...17
2.3.1 Energy conversion efficiency…………………………………………18
2.3.2 Short circuit current…………………………………………………...18
2.3.3 Open circuit voltage (V_{oc})…………………………………………19
2.3.4 Fill factor………………………………………………………………21
2.4 Application of heterojunction solar cells or window effect…….…………21

CHAPTER III: RESEARCH METHODOLOGY…………………………………24
3.1 General………………………………………………………………..24
3.2 Literature review……………………………………………………...24
3.3 Experimental Data Correction…….…………………………………..24
3.3.1 Liquid phase epitaxy (LPE)…………………………………......24

3.3.2 Molecular beam epitaxy (MBE)……………………………………….27
3.3.2.1 The MBE system……………………………………………...27
3.3.2.2 In-situ characterization tools……………………………………34
3.3.3 Photoluminescence (PL)……………………………….………...36
3.4 GaAs and AlGaAs for LPE………….……..…………………………...37
3.4.1 Material preparation…………………………………………………...37
3.4.2 Material weight calculation…………………………………………...41
3.5 Growth process…………………...……………………………………...43
3.5.1 Liquid phase epitaxy……………………………………………….…43
3.5.2 Molecular beam epitaxy……………………………………………46

CHAPTER IV: EXPERIMENTAL RESULT AND DISCUSSION..……………49
4.1 General…………………………………………………………………..49
4.2 Heterostructure Solar cells realization…..…………...……………………..49
4.2.1 MBE samples………………………………………………………49
4.2.2 LPE samples……………………………………………………...54
4.3 Results and discussion…………………………………………………...…55

CHAPTER V: CONCLUSIONS……………………………………………….69
5.1 Heterostructure solar cells…………………………………………………69
5.2 Limitation of study…………………………………………………………69
5.3 Further study………………………………………………………………69
REFERENCES……………………………………………………………………70
BIOGRAPHY……………………………………………………………………...72

ศูนย์วิทยทรัพยากร
จุฬาลงกรณ์มหาวิทยาลัย

LIST OF FIGURES

Figure 1.1 Amount of energy in the sunlight reaching the Earth's surface is equivalent to around 10,000 times the world's energy requirements. Consequently, only 0.01 per cent of the energy in sunlight would need to be harnessed to cover mankind’s total energy needs …………………………………………………………………..2

Figure 2.1 Schematic illustration of 2 dimensional crystal structure **(a)** and band diagram of n type and p type semiconductors **(b)**……………………………………7

Figure 2.2 Schematic of n-p junction structure **(a)** and energy band diagram **(b)**……8

Figure 2.3 Structure and energy band of solar cell………………………………..10

Figure 2.4 Energy band diagram and schematic structure of (a) Schottky barrier, and (b) MIS solar cell……………………………………...……………………...15

Figure 2.5 Calculation result of collection efficiency of schottky barrier solar cell...16

Figure 2.6 Structure of solar cells where n-type energy band diagram is greater than p-type……………………………………………………………………………17

Figure 2.7 Equivalent circuits of solar cells…………………………………………19

Figure 2.8 Maximum outputs of solar cells………………………………….…20

Figure 2.9 Band diagrams of AlGaAs/GaAs homojunction solar cells……………...22

Figure 3.1 Horizontal LPE systems…………………………………………………25

Figure 3.2 Multi-bin graphite boats…………………………………………………26

Figure 3.3 **(a)** diagram of growth chamber and **(b)** schematic illustration of a RIBER 32P MBE system…………………………………………………………………..28

Figure 3.4 Temperature profile of the pre-heat process…………………………..30

Figure 3.5 Temperature of Ga and In effusion cells. The effusion cell is closed in the dotted line range and opened in solid line range during respective temperature ranges…………………………………………………………………………...31

Figure 3.6 Temperature profile of As effusion cell and substrate. The effusion is closed in the dotted line range and opened in solid line range during respective temperature ranges…………………………………………………………...31

Figure 3.7 **(a)** temperature profile of the oxide desorption process and RHEED pattern when the temperature increases and **(b)** photo took from view port showing RHEED spotty pattern at de-oxide temperature at 580°C……………………………33

Figure 3.8 Schematic diagram of mass spectrometer... 34

Figure 3.9 Schematic diagram presentation of RHEED geometry shows incident electron beam at an angle Θ to the surface plane……………………………………….36
Figure 3.10 Schematic diagram of PL experiment set up…………………………...36
Figure 3.11 Liquidus composition versus reciprocal temperature for GaAs, GaP and InP…………………………………………………………………………………39
Figure 3.12 Room temperature hole concentration in GaAs versus the atom fraction of Ge in the liquid along the 800 and 900°C and the lower curves are the room temperature electron concentration in GaAs versus the atom fraction of Sn in the liquid along the 700 and 800°C………………………………………………………39
Figure 3.13 Solidus compositions in $Al_xGa_{1-x}As$ as a function of liquidus composition……………………………………………………………………………..40
Figure 3.14 Liquidus isotherms in the AlGaAs system……………………………..40
Figure 3.15 **(a)** Basic set up of LPE system, **(b)** and **(c)** schematic profile of the furnace temperature versus the growing time duration, samples **G** and **H**…………..45
Figure 4.1 Schematic diagrams of Schottky heterostructure solar cells (sample **A**)...50
Figure 4.2 Schematic diagram of heterojunction solar cells with fixed Al content of 0.3 (sample **B**)……………………………………………………………………….…51
Figure 4.3 Schematic diagram of heterojunction solar cell having $Al_xGa_{1-x}As$ window with stepped Al mole fractions (sample **C**)…………………………………52
Figure 4.4 Schematic diagram of heterojunction solar cell, the $Al_xGa_{1-x}As$ window with a stepped Al mole fraction having thin 200nm GaAs buffer layer (sample **D**)...52
Figure 4.5 Schematic diagram of heterojunction solar cell, the $Al_xGa_{1-x}As$ window with a stepped Al mole fraction (sample **E**)…………………………………………53
Figure 4.6 Schematic diagram of heterojunction solar cell, the $Al_xGa_{1-x}As$ window with a stepped Al mole fraction (sample **F**)…………………………………………53
Figure 4.7 **(a), (b)** Schematic diagram of the heterostructure solar cells, (sample **G** and **H**) grown by LPE technique……………………………………………………..54
Figure 4.8 **(a), (b)** and **(c)** Spectral responses of samples **A, B** and **C**………………57
Figure 4.9 Normalized spectral responses of samples **B** and **C**……………………..57
Figure 4.10 **(a), (b)** and **(c)** Spectral responses of samples **D, E** and **F**……………..59
Figure 4.11 Normalized spectral responses of samples **D, E** and **F**…………………59
Figure 4.12 **(a), (b)** and **(c)** Photoluminescence of samples **A, B** and **C,** respectively……………………………………………………………………………...61

Figure 4.13 (a), (b), (c), (d) and **(e)** I-V curves in dark and one sun of AlGaAs/GaAs heterostructure solar cells, samples **B**, **C, D, E** and **F** respectively…………………..63

Figure 4.14 (a) Spectral responses of sample **G**, **(b)** Spectral responses of sample **H** and **(c)** normalized spectral responses of sample **G** and **H**…………………………..65

Figure 4.15 (a) and **(b)** I-V curves in the dark and one sun of AlGaAs/GaAs heterostructure solar cells, sample **G** and **H** respectively**…**…………………………66

ศูนย์วิทยทรัพยากร
จุฬาลงกรณ์มหาวิทยาลัย

LIST OF TABLES

Table 2.1 lattice mismatch and band discontinuity of semiconductor that we make the heterojunction anisotype…………………………………………………………..23

Table 3.1 Material weight……………………………………………………………43

Table 4.1 Solar cell parameters of samples **B, C, D, E** and **F**………………………64

Table 4.2 The calculated solar cell's output parameters of sample **G** and **H**………..67

ศูนย์วิทยทรัพยากร
จุฬาลงกรณ์มหาวิทยาลัย

CHAPTER I
INTRODUCTION

1.1 Introduction

Any discussion of solar energy and solar (photovoltaic) cells should begin with an examination of the energy source, the sun. Our sun is a dG2 star, classified as a yellow dwarf of the fifth magnitude. The sun has a mass of approximately 10^{24} tons, a diameter of 865,000 miles, and radiates energy at a rate of some 3.8 x 10^{20} megawatts. Present theories predict that this output will continue, essentially unchanged, for several billion years. It is necessary to say essentially, because the sun's energy output may fluctuate by a few percent from time to time **[1]**. The sun supplies energy in the form of radiation, without which life on Earth could not exist. The energy is generated in the sun's core through the fusion of hydrogen atoms into helium. Part of the mass of the hydrogen is converted into energy. In other words, the sun is an enormous nuclear fusion reactor. Because the sun is such a long way from the Earth, only a tiny proportion (around two-millionths) of the sun's radiation reaches the Earth's surface. This works out at an amount of energy of 1 x10^{18} kWh/area. The **figure 1.1** compares this amount of energy to worldwide annual energy consumption and to fossil and nuclear energy resources. The energy sources that we primarily use in our industrial age are exhaustible. A supply shortage (from the technical and economic points of view) in easily extractable oil and natural gas reserves is anticipated in the first third of this century. Even if large new reserves were discovered, fossil fuels would still only last for a few more years. The amount of energy in the sunlight reaching the Earth's surface is equivalent to around 10,000 times the world's energy requirements. Consequently, only 0.01 per cent of the energy in sunlight would need to be harnessed to cover mankind's total energy needs **[2]**.

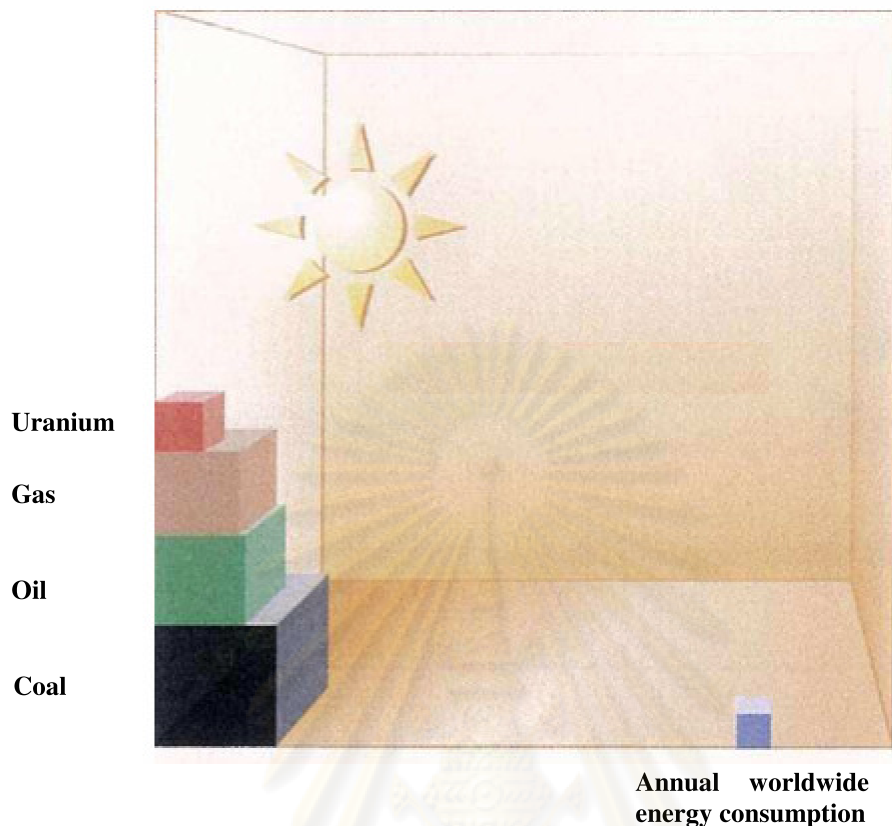

Figure 1.1 Amount of energy in the sunlight reaching the Earth's surface is equivalent to around 10,000 times the world's energy requirements. Consequently, only 0.01 per cent of the energy in sunlight would need to be harnessed to cover mankind's total energy needs **[2]**.

Photovoltaic energy conversion in solar cells consists of two essential steps. First, absorption of light generates an electron-hole pair. The electron and hole are then separated by the structure of the device - electrons to the negative terminal and holes to the positive terminal - thus generating electrical power. The effectiveness of a photovoltaic device depends upon the choice of light absorbing materials and the way in which they are connected to the external circuit **[3]**. The first functional, intentionally made PV device was by Fritts in 1883. He melted Se into a thin sheet on a metal substrate and pressed a Au-leaf film as the top contact. It was nearly 30 cm^2 in area. He noted, "the current, if not wanted immediately, can be either stored where produced, in storage batteries, . . . or transmitted a distance and there used." This man

foresaw today's PV technology and applications over a hundred years ago. The modern era of photovoltaics started in 1954 when researchers at Bell Labs in the USA accidentally discovered that *pn* junction diodes generated a voltage when the room lights were on. Within a year, they had produced a 6% efficient Si *p-n* junction solar cell **[4]**. In the same year, the group at Wright Patterson Air Force Base in the US published results of a thin-film heterojunction solar cell based on Cu_2S/CdS also having 6% efficiency **[5]**. A year later, a 6% GaAs *p-n* junction solar cell was reported by RCA Lab in the US **[6]**. By 1960, several key papers by Prince, Loferski, Rappaport and Wysoski , Shockley (a Nobel laureate) and Queisser, developed the fundamentals of *pn* junction solar cell operation including the theoretical relation between band gap, incident spectrum, temperature, thermodynamics, and efficiency. Thin films of CdTe were also producing cells with 6% efficiency. By this time, the US space program was utilizing Si PV cells for powering satellites. Since space was still the primary application for photovoltaics, studies of radiation effects and more radiation-tolerant devices were made using Li-doped Si. In 1970, a group at the Ioffe Institute led by Alferov (a Nobel laureate), in the USSR, developed a heteroface GaAlAs/GaAs solar cell which solved one of the main problems that affected GaAs devices and pointed the way to new device structures. GaAs cells were of interest due to their high efficiency and their resistance to the ionizing radiation in outer space. The year 1973 was pivotal for photovoltaics, in both technical and nontechnical areas. A significant improvement in performance occurring in 1973 was the "violet cell" having an improved short wavelength response leading to a 30% relative increase in efficiency over state-of-the-art Si cells. GaAs heterostructure cells were also developed at IBM in the USA having 13% efficiency **[7]**.

In the 1970s and 1980s, high efficiency and improved radiation hardness of the AlGaAs/GaAs solar cells stimulated the large-scale production of AlGaAs/GaAs space arrays for spacecrafts. An AlGaAs/GaAs solar cell with total area of 70m^2 was installed in the Russian space station MIR launched in 1986. During 15 years in orbit, the array degradation appeared to be lower than 30% under conditions that included appreciable shadowing, the effects of numerous docking, and a challenging ambient environment. At that time, it was the best large-scale demonstration of AlGaAs/GaAs

ศูนย์วิทยทรัพยากร
จุฬาลงกรณ์มหาวิทยาลัย

solar cell advantages for space application. Further improvement of the LPE technology allowed obtaining the efficiency of 24.6% (AM0, 100 suns) on the basis of the heterostructures with an ultra-thin AlGaAs window layer and the back surface flied layer **[8].**

1.2 Problem Statements

(1) To study fundamental definition of solar cell such as the materials, the structure and optical properties.

(2) To research and to fabricate the solar cell focusing on AlGaAs/GaAs heterostructure solar cell, and then to evaluated the sample by photoluminescence, spectral response, and I-V curve measurement.

(3) To propose and to increase the research of solar cells in developing country such as my country, Laos.

1.3 Objective

The main objectives of this research are:

(1) To study fundamental properties of AlGaAs and GaAs material system.

(2) To fabricate AlGaAs/GaAs heterostructure solar cells.

(3) To characterize AlGaAs/GaAs heterostructure solar cells.

1.4 Scope of Research

(1) To study fundamental of solar cell structure, and how solar cells work.

(2) To study methodology of fabrication.

(3) To fabricate AlGaAs/GaAs heterostructure solar cells.

(4) To characterize by photoluminescence, I-V curve and spectral response.

(5) To calculate fill factor, and efficiency.

1.5 Research Methodology

(1) Literature review on fundamental of solar cells for understanding.

(2) Literature review on AlGaAs/GaAs solar cells.

(3) Design and fabricate AlGaAs/GaAs heterostructure solar cells.

(4) Measure the electrical and optical properties of Heterostructure solar cells.

1.6 Expected Benefits

The future benefit of this study can be:

(1) To give me the basic knowledge of solar cells, and the technical know-how in fabricating AlGaAs/GaAs heterostructure solar cells.

(2) To gain knowledge in characterization of optical, and electrical properties of the solar cell.

(3) To be useful in knowledge transfer to my country especially to National University of Laos, Faculty of Engineering, and Department of Electronic Engineering.

CHAPTER II
FUNDAMENTAL OF SOLAR CELL

2.1 General

The objective of this chapter is mainly to elaborate on the knowledge and competencies of solar cells from many previous researchers who studied about the solar cells. Various researches were especially conducted in heterojunction solar cells, and most of them mostly delineated the knowledge and competencies of solar cells.

2.2 Fundamental definition, and operation of solar cells

To understand the photovoltaic effect, some basic theory about semiconductors and their use as photovoltaic energy conversion devices needs to be given as well as information on p-n junction **[7]**. The term photovoltaic means the direct conversion of light into electrical energy using solar cells. Semiconductor materials such as Silicon, Gallium Arsenide, Cadmium Telluride or Copper Indium Diselenide are used in these solar cells **[7]**.

The semiconductor described so far is intrinsic; it is a perfect crystal containing no impurity. The one which has been doped to increase the density of electrons relative to holes is n-type semiconductor, and the one which is doped to increase the density of positive charge carriers relative to negative charge is p-type semiconductor. The schematic illustration of 2 dimensional structures of n and p type semiconductors and energy band diagram are shown in **figure 2.1 (a)** and **(b)**.

ศูนย์วิทยทรัพยากร
จุฬาลงกรณ์มหาวิทยาลัย

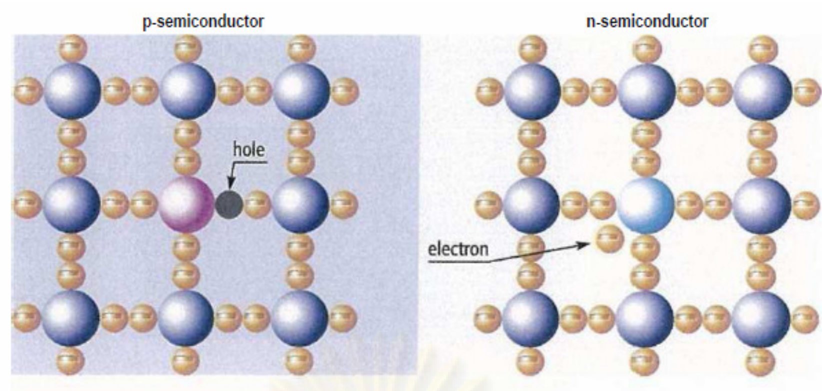

(a)

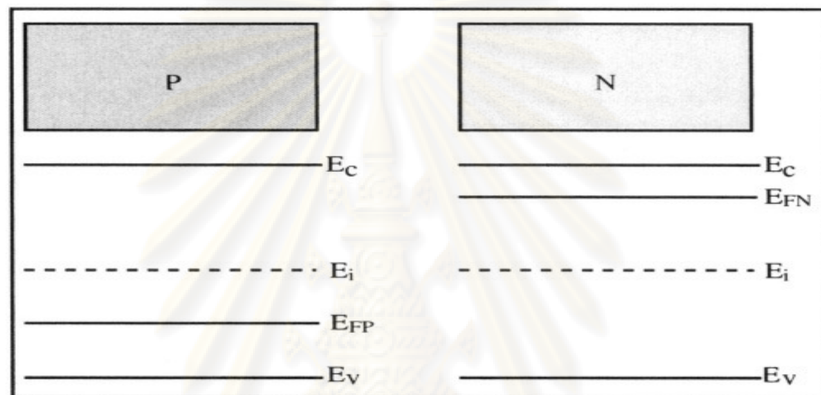

(b)

Figure 2.1 Schematic illustration of 2 dimensional crystal structure **(a)** and band diagram of n type and p type semiconductors **(b)** **[2]**.

The structure of solar cells is a p-n junction, as shown in **figure 2.2**. If the n- and p-type region is the same semiconductor material, the junction is a homojunction. If the semiconductor is different, we call heterojunction **[9]**.

ศูนย์วิทยทรัพยากร
จุฬาลงกรณ์มหาวิทยาลัย

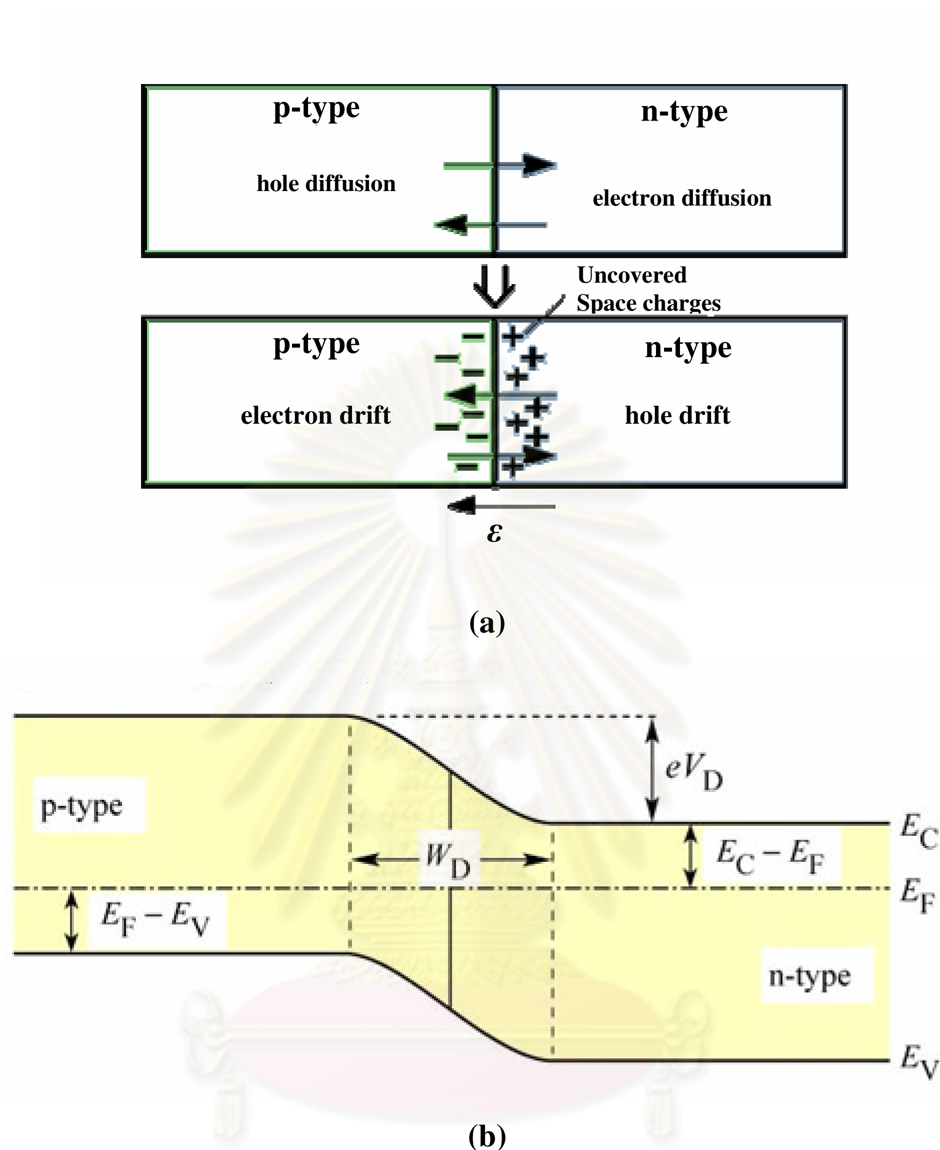

Figure 2.2 Schematic of n-p junction structure **(a)** and energy band diagram **(b) [2].**

2.2.1 Spectral response and collection efficiency

The photon is incident on solar cell panel, and then the solar cell generates the photocurrent. The photocurrent depends both on the spectral response of solar cell and spectral radiation of sunlight.

Spectral response is the rate of short circuit current J_{sc} (λ) per photon energy P (λ) absorbed by the panel, J_{sc} (λ) and P (λ) are the function of sunlight wavelength. The unit of spectral response is ampere per watt (A/W).

Collection efficiency is the amount of electrons that solar cells generate per amount of the photon absorbed.

There are two definition of collection efficiency:

(1) Internal collection efficiency, η_{in}.

In the case, there is no reflection from the solar cells panel.

(2) External collection efficiency, $\eta_{ext.}$

In the case, there is reflection from solar cells panel.

We can write the internal and external collection efficiency.

$$\eta_{In}(\lambda) = \frac{Jsc(\lambda)}{P(\lambda)} = \frac{Jsc(\lambda)}{qF(\lambda)[1 - R(\lambda)]} \qquad \textbf{(2.1)}$$

$$\eta_{Ext}(\lambda) = \eta_{In}(\lambda)[1 - R(\lambda)] = \frac{Jsc(\lambda)}{qF(\lambda)} \qquad \textbf{(2.2)}$$

R (λ): Reflection index of photon at solar cell surface.

F (λ): Photon flux, amount of photon per unit area and time unit is access on the cells.

q: Electron charge.

Actually, internal collection efficiency is greater than external collection efficiency, and both of them are less than one. Almost of external collection efficiency can calculate from **(2.2)**.

$$\eta_{Ext} = \frac{\sum Jsc(\lambda)}{q\sum F(\lambda)} \qquad \textbf{(2.3)}$$

- **Collection Efficiency of p-n Junction Solar Cells**

We consider the collection efficiency of p-n junction solar cells as shown in the **figure 2.3**. Collection efficiency can be calculated by separating the layer of solar

cells, n, depletion and p layer from each other; and short circuit current is calculated by solving diffusion equation.

In steady state, continuity equation of minority carrier hole is generated by photon in n-type in written as.

$$\frac{dJ_h}{dx} + \frac{Pn - Pno}{q\tau_h} - g(x) = 0 \tag{2.4}$$

$$J_h = q\mu_h p_n E - qD_h \frac{dp_n}{dx} \tag{2.5}$$

Continuity equation of minority carrier electron is generated by photon in p type is written as.

$$\frac{dJ_e}{dx} - \frac{n_p - n_{no}}{q\tau_e} + g(x) = 0 \tag{2.6}$$

$$J_e = q\mu_e n_p E + qD_e \frac{dn_p}{dx} \tag{2.7}$$

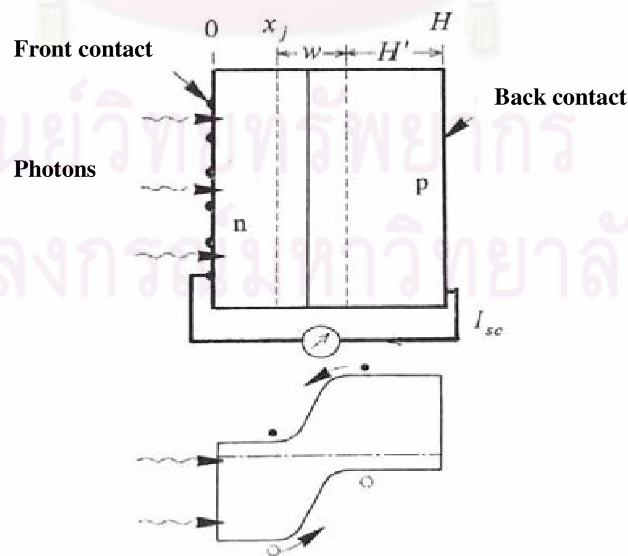

Figure 2.3 Structure and energy band of solar cell **[10]**.

J_e: Current of electron per unit area.

J_h: Current of hole per unit area.

τ_e: Lifetime of electron.

n_p: Number of electron per unit area in p layer.

D_e: Diffusion coefficient of electron.

g(x): generation rate of carrier per second.

q: Electron charge.

E: Electric field.

μ_e: Mobility of electron.

μ_h: Mobility of hole.

τ_h: Lifetime of hole.

p_n: Number of hole per unit area in n layer.

D_h: Diffusion coefficient of hole.

p_{n0}, n_{p0}: Carrier concentration at thermal equilibrium.

x: Distance from surface.

To solve equation of **2.4 ~2.7,** we will set up boundary condition as follow

$$p_n = p_{no}\exp(qV/kT) \quad \text{, at } x = x_J \qquad \textbf{(2.8)}$$

$$n_p = n_{po}\exp(qV/kT) \quad \text{, at } x = x_J + w \qquad \textbf{(2.9)}$$

$$S_h(p_n - p_{no}) = D_h\frac{dp_n}{dx} - \mu_h p_n E \quad \text{, at } x = 0 \qquad \textbf{(2.10)}$$

$$S_e(n_p - n_{po}) = D_e\frac{dn_p}{dx} - \mu_e n_p E \quad \text{, at } x = H \qquad \textbf{(2.11)}$$

S_e: Recombination velocity of electron at solar cells surface (x=H).

S_h: Recombination velocity of hole at solar cells surface.

W: Width of depletion layer.

In depletion layer, there are built-in potential generates from space charge, but in p and n layer, there are less built-in potential. If we are not considered the built-in potential in p and n, we can write the continuity equation in n layer by equation of **2.4** and **2.5**:

$$D_h \frac{d^2 p_n}{d x^2} + g(x) - \frac{p_n - p_{no}}{\tau_h} = 0 \tag{2.12}$$

$$g(x) = \alpha F(1-R)\exp(-\alpha x) \tag{2.13}$$

Then we solve the equation of **2.12**

$$p_n - p_{no} = A Cosh \frac{x}{L_h} + B \sinh \frac{x}{L_h} - \frac{\alpha F(1-R)\tau_h}{\alpha^2 L_h^2 - 1}\exp(-\alpha x) \tag{2.14}$$

L_h: Diffusion distance of hole, $L_h = (D_h \tau_h)^{1/2}$.

α: Absorption coefficient.

R: Reflection coefficient.

A and B can calculate by two conditions:

1 $x = x_J$, there are negligible excess carriers

$$p_n - p_{no} = 0, \quad x = x_j \tag{2.15}$$

2 On the front surface of solar cells, there is recombination.

$$D_h \frac{d(p_n - p_{no})}{dx} = S_h (p_n - p_{no}), \quad x = 0 \tag{2.16}$$

After giving two conditions, we can write the equation of **2.14**.

$$P_n - P_{no} = \left[\frac{\alpha F(1-R)\tau_h}{\alpha^2 L_l^2 - 1}\right]\left[\frac{\left(\frac{S_h L_h}{D_h} + \alpha L_h\right) Sinh \frac{x_J - x}{L_h} + \exp(-\alpha x_J)\left(\frac{S_h L_h}{D_h} Cosh \frac{x_J}{L_h} + Sinh \frac{x_J}{L_h}\right)}{\frac{S_h L_h}{D_h} Sinh \frac{x_J}{L_h} + Cosh \frac{x_J}{L_h}} - \alpha L_h \exp(-\alpha x_J)\right] \tag{2.17}$$

$x = x_j$ is the edge of depletion layer. Photocurrent of hole (J_h) generates in n layer.

$$J_h = -q D_h \frac{d p_n}{dx}$$

$$= \left[\frac{qF(1-R)\alpha L_h}{\alpha^2 L_h^2 - 1}\right]\left[\frac{\frac{S_h L_h}{D_h} + \alpha L_h - \exp(-\alpha x_J)\left(\frac{S_h L_h}{D_h} Cosh \frac{x_J}{L_h} + Sinh \frac{x_J}{L_h}\right)}{\frac{S_h L_h}{D_h} Sinh \frac{x_J}{L_h} + Cosh \frac{x_J}{L_h}} - \alpha L_h \exp(-\alpha x_J)\right] \quad \textbf{(2.18)}$$

In the same case, photocurrent of electron (J_e) generates in n layer can be calculated from equation of **2.16** and **2.17** by giving two conditions.

1 $n_p - n_{po} = 0, \quad x = x + w$ **(2.19)**

2 $-D_e \frac{d(n_p - n_{po})}{dx} = S_e(n_p - n_{po})$, x = H **(2.20)**

From two conditions, we get J_e:

$$J_e = q D_e \frac{d n_p}{dx} = \frac{qF(1-R)\alpha L_e}{\alpha^2 L_e^2 - 1} \exp[-\alpha(x_J + w)]$$

$$\times \left[\alpha L_e - \frac{\frac{S_e L_e}{D_e} Cosh \frac{H'}{L_e} - \exp(-\alpha H')) + Sinh \frac{H'}{L_e} + \alpha L_e \exp(-\alpha H')}{\frac{S_e L_e}{D_e} Sinh \frac{H'}{L_e} + Cosh \frac{H'}{L_e}}\right] \quad \textbf{(2.21)}$$

For $H' = H - (x_J + w)$

From equation of **2.18** and **2.21**, we get “the value of photocurrent of hole (J_h) and electron (J_e) correspond to absorption coefficient of photon (α) and diffusion distance of carriers (L_e, L_h)”.

Next, we consider the photocurrent generates in depletion layer. The carrier is excited in depletion layer, and pull out of the external by electric field of p-n junction. Those carriers are not recombined or recombine a little. The current flow like this, called drift current (J_{dr}).

$$J_{dr} = qF(1-R)\exp(-\alpha x_J)[1 - \exp(-\alpha w)] \quad \textbf{(2.22)}$$

W: depletion thickness.

ศูนย์วิทยทรัพยากร
จุฬาลงกรณ์มหาวิทยาลัย

$$w = \left[\frac{2\varepsilon_s}{q} (v_d - v) \frac{N_a - N_d}{N_a N_d} \right]^{1/2} \quad \textbf{(2.23)}$$

ε_s: Dielectric permittivity of semiconductor.

N_a, N_d: Density of acceptor, donor impurity atoms.

V_d: Voltage generates from p-n junction.

V: Bias voltage.

We can summarize, the short circuit photocurrent at each wavelength of photon in p-n junction ($J_{sc}(\lambda)$).

$$J_{sc} = J_h(\lambda) + J_e(\lambda) + J_{dr}(\lambda) \quad \textbf{(2.24)}$$

η_{in} and η_{ext} can be calculated from equation of **2.1** and **2.2**. This equation can be used the photon access on the n layer. The photon access on the p layer also can be used, but there have to change the subscription **[10]**.

- **Collection efficiency of Schottky barrier and MIS (Metal Insulator Semiconductor) solar cells**

Figure 2.4 (a) and (b) demonstrate schematic structure and energy band diagram of Schottky barrier and MIS solar cells. Both of them, the access photon of the metal layer tunnels to semiconductor layer. Therefore, the carrier is excited by photon at depletion and semiconductor layer. So the photocurrent generates at depletion region is the same equation **2.22**

$$J_{dr} = qT(\lambda)F(\lambda)\left[1 - \exp(-\alpha w)\right] \quad \textbf{(2.25)}$$

T(λ): tunneling metal layer coefficient/Insulator of photon.

W: depletion thickness.

$$W = \left[\frac{2\varepsilon_s}{qN_d} \left(V_d - V \right) \right]^{1/2} \quad \textbf{(2.26)}$$

Next semiconductor layer generates photocurrent of holes.

$$J_h = \left(\frac{qF\alpha L_h}{\alpha L_h + 1} \right) T(\lambda) \exp(-\alpha w) \quad \textbf{(2.27)}$$

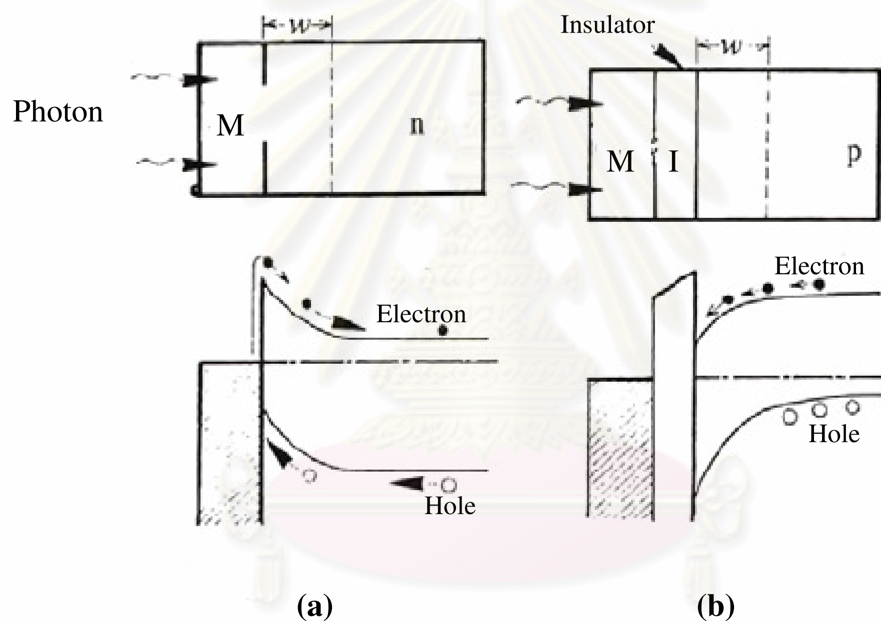

Figure 2.4 Energy band diagram and schematic structure of (a) Schottky barrier, and (b) MIS solar cell **[11]**.

To suppose that $\alpha L_h >> 1$

$$J_{sc}(\lambda) = J_{dr}(\lambda) + J_h(\lambda)$$

$$= T(\lambda) qF(\lambda) \left[1 - \exp(-\alpha w) \frac{\alpha L_h}{\alpha L_h + 1} \right] \quad \textbf{(2.28)}$$

ศูนย์วิทยทรัพยากร จุฬาลงกรณ์มหาวิทยาลัย

Therefore, the collection efficiency $\eta_{In}(\lambda)$.

$$\eta_{In}(\lambda) = \frac{J_{sc}(\lambda)}{qF(\lambda)T(\lambda)} \tag{2.29}$$

Figure 2.5 shows the calculation of collection efficiency (η_{In}) of Schottky barrier solar cells. There is a bit influence from carrier recombination on the front surface. So collection efficiency of schottky barrier is greater than p-n junction **[11]**.

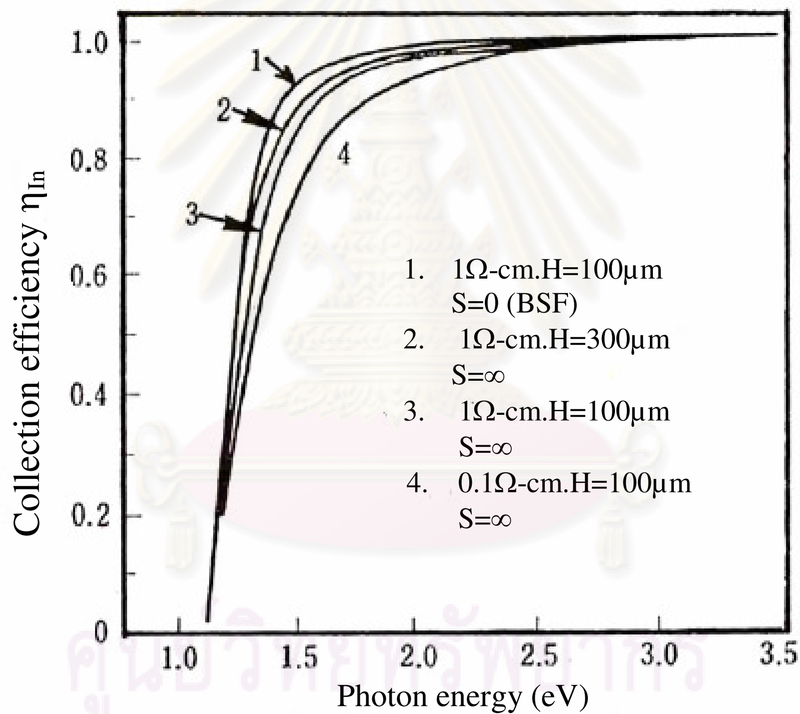

Figure 2.5 Calculation result of collection efficiency of schottky barrier solar cell **[11]**.

- **Collection efficiency of heterojunction solar cells**

Heterojunction solar cells are consisting of two different energy band semiconductors being contacted to be a p-n junction. **Figure 2.6** shows the sample of

p-n heterojunction solar cells; n-type energy band diagram is wider than p-type, and the photon accesses on n-type surface. The carrier generates in p-type is more influence to efficiency. The electron current generates in p-type layer can be calculated from the equation **(2.6), (2.7), (2.9)** and **(2.20)**, by consideration some part of photon being absorbed in n-type.

$$J_e(\lambda) = \frac{qF(\lambda)\exp\left[-\alpha(x_j + w_1)\right]\exp(-\alpha_2 w_2)\alpha_2 L_{e2}(1-R)}{\alpha_2^2 L_{e2}^2 - 1} \times$$
$$\left[\alpha_2 L_{e2} - \frac{\frac{S_e L_{e2}}{D_{e2}}\left(\cosh\frac{H'}{L_{e2}} - ex(-\alpha H')\right) + \sinh\frac{H'}{L_{e2}} + \alpha_2 L_{e2}\exp(-\alpha H')}{\frac{S_e L_{e2}}{D_{e2}}\sinh\frac{H'}{L_{e2}} + \cosh\frac{H'}{L_{e2}}} \right] \quad \textbf{(2.30)}$$

In this p-n heterojunction, there are two depletion regions w_1 and w_2 as shown in **figure 2.6**. Hole current is generated in n-type layer, calculates by using equation **2.18**. And $J_{dr}(\lambda)$ equal to $J_{w1}+J_{w2}$, J_{w1} can be calculated by equation **2.22** and J_{w2} also can be calculated by equation **2.22** but using x_j+w_1 instead of x_j.

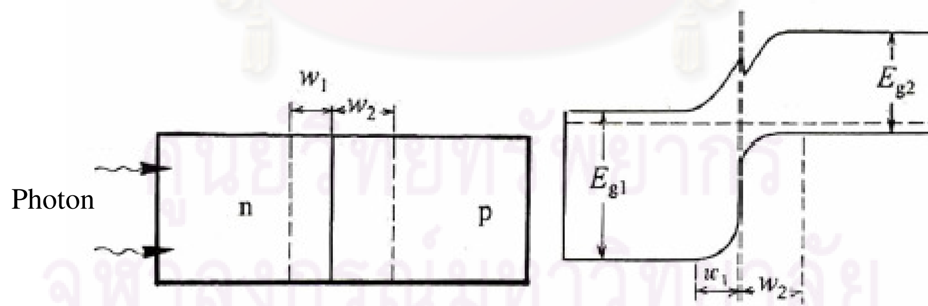

Figure 2.6 Structure of solar cells where n-type energy band diagram is greater than p-type **[11]**.

2.3 Output characteristics of solar cells

The following electrical and optical characteristics are used to explain the performance of solar cells.

2.3.1 Energy conversion efficiency

It means the ratio between maximum output power per sunlight energy incident on the solar cells and simply written by η.

$$\eta = \frac{P_{\max}(w)}{Area(m^2) \times P_{in}(w)} \times 100\% \quad \textbf{(2.31)}$$

2.3.2 Short circuit current

If solar cells output terminals are in short circuit, we call the current flows on the circuit "Short circuit current (I_{sc})".

Figure 2.7 demonstrates the equivalent circuit of solar cells. If the solar cells is in the dark, the relation between dark current (I) and voltage (V) of solar cells is the same as the current equation of diode.

$$I = I_o\left[\exp(qV / nkT) - 1\right] \quad \textbf{(2.32)}$$

$$I_0 = qA\left[\frac{D_h P_n}{L_h} + \frac{D_e n_p}{L_e}\right]$$

I_0 is called saturation current and n is ideality factor of diode.

So I_{out} flows to external, this current is different between dark current I and I_{ph} (=I_{sc}).

$$I_{out} = I - I_{ph} \quad \textbf{(2.33)}$$

I_{ph}(=I_{sc}) from equation of **2.2**, A is area of the photon access.

$$I_{sc} = qA\int_0^{\infty} F(\lambda)\eta_{ext}(\lambda)d\lambda \qquad \textbf{(2.34)}$$

To consider the resistance inside of solar cells such as series resistance (R_s) and shunt resistance (R_{sh}), so we can write I_{out}.

$$I_{out} = I_0\{\exp\left[\frac{q(V-IRs)}{nkT}\right]-1\} + \frac{V-IRs}{R_{sh}} - I_{ph} \qquad \textbf{(2.33')}$$

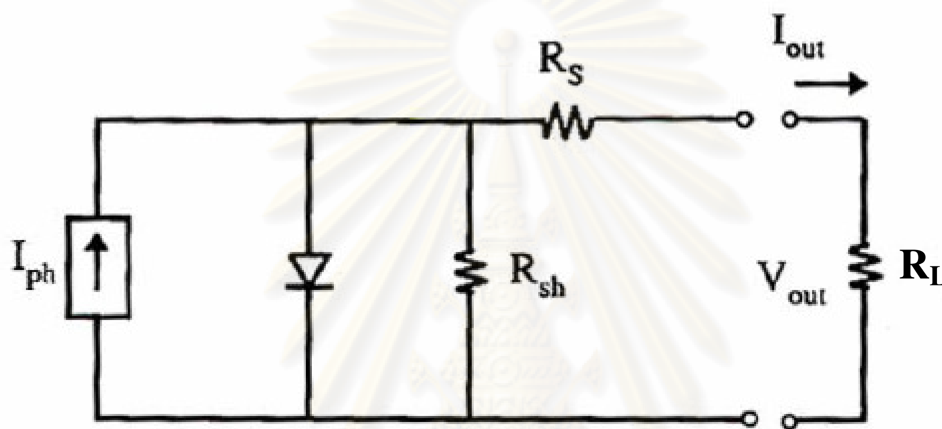

Figure 2.7 Equivalent circuits of solar cells **[12]**.

2.3.3 Open circuit voltage (V_{oc})

If output of solar cells is in open circuit, the voltage that we measure, calls "Open circuit voltage (V_{oc})". V_{oc} can be calculated from equation of **2.33** by giving I_{out} = 0.

$$V_{oc} = \frac{nkT}{q}\ln(\frac{I_{sc}}{I_0}+1) \qquad \textbf{(2.35)}$$

The **figure 2.8** demonstrates the output characteristics of solar cells. The point of graph intersect voltage axis, is called open circuit voltage (V_{oc}). The point of graph intersect current axis, is called short circuit current (I_{sc}). Then the maximum power (P_{max}) is equal to the area of square being calculated by V_{max} and I_{max}. On the **figure**

ศูนย์วิทยทรัพยากร
จุฬาลงกรณ์มหาวิทยาลัย

2.8 also shows the parameter of maximum voltage (V_{max}), and maximum current (I_{max}).

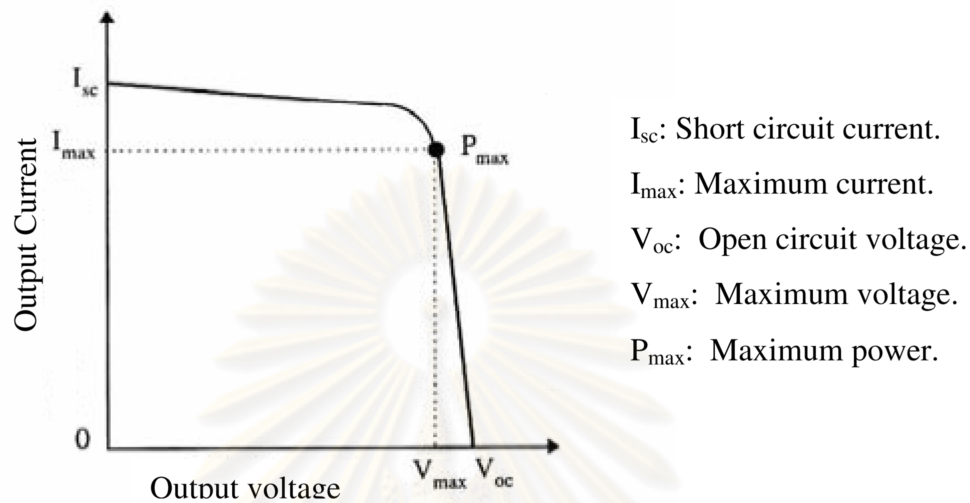

Figure 2.8 Maximum outputs of solar cells **[12]**.

$$P_{max} = V_{max} \times I_{max} \quad \textbf{(2.36)}$$

We can calculate V_{max} by finding the derivative of maximum power (P_{max}) with respect to maximum voltage (V_{max}) and let

$$\frac{\partial P_{max}}{\partial V_{max}} = 0$$

The solution is

$$\exp\left(\frac{qV_{max}}{nkT}\right)\left(1+\frac{qV_{max}}{nkT}\right) = \left(\frac{I_{sc}}{I_0}+1\right) \quad \textbf{(2.37)}$$

It is the same case, we can calculate maximum current (I_{max}).

$$I_{max} = \frac{(I_{sc}+I_0)\frac{qV_{max}}{nkT}}{1+\frac{qV_{max}}{nkT}} \quad \textbf{(2.38)}$$

ศูนย์วิทยทรัพยากร
จุฬาลงกรณ์มหาวิทยาลัย

2.3.4 Fill Factor

An other important output parameter is the fill factor which is defined as ratio between $V_{max} \times I_{max}$ and $V_{oc} \times I_{sc}$.

$$FF = \frac{P_{max}}{V_{oc} \times I_{sc}} = \frac{V_{max} \times I_{max}}{V_{oc} \times I_{sc}} \tag{2.39}$$

$$= \frac{V_{max}}{V_{oc}} \left[1 - \frac{\exp(qV_{max} / nkT) - 1}{\exp(qV_{oc} / nkT) - 1} \right] \tag{2.40}$$

If series resistance (R_s) is less, the fill factor (FF) is great.

If we know the parameter output above, we calculate the efficiency of solar cells.

$$\eta = \frac{P_{max}}{P_{in}} \times 100\% = \frac{V_{max} \times I_{max}}{P_{in}} = \frac{V_{oc} \times I_{sc} \times FF}{P_{in}} \times 100\% \tag{2.41}$$

$$= FF \times (nkT / q) \ln[(I_{sc} / I_0) + 1] \times q \times \frac{\int_0^\infty F(\lambda) \eta_{ext}(\lambda) d\lambda}{\int_0^\infty F(\lambda) \times (hc / \lambda) d\lambda} \tag{2.42}$$

2.4 Application of heterojunction solar cells or window effect

The junction which is made form two different type semiconductors called heterojunction. If two type of semiconductors is the same such as n-n and p-p, called isotype junction. Otherwise, if they are different such as p-n or n-p, called anisotype.

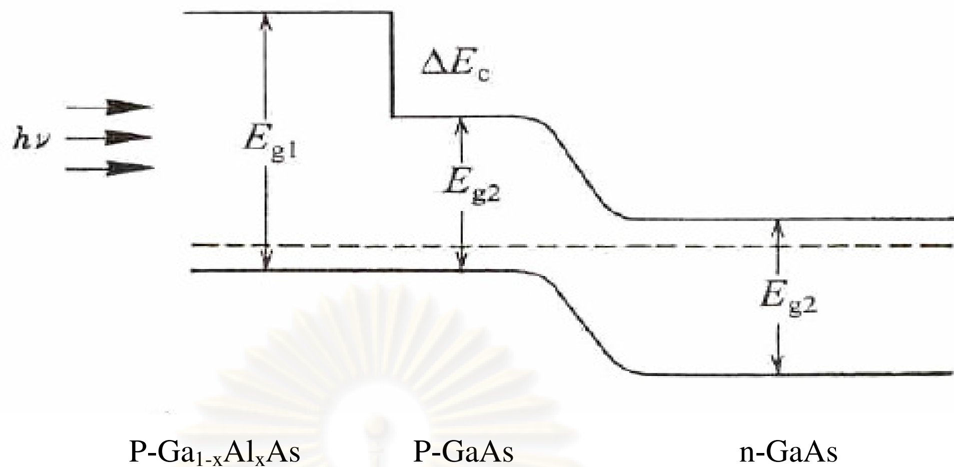

Figure 2.9 Band diagrams of AlGaAs/GaAs homojunction solar cells **[12]**.

Isotype junction is more important for homojunction solar cells. **Figure 2.9** demonstrates solar cells band diagram of p-$Ga_{1-x}Al_xAs$/p-GaAs/n-GaAs. If there is no layer of p-$Ga_{1-x}Al_xAs$, the rate recombination of electrons of solar cells at p-GaAs surface will be greater than 10^6 cm/s. So there is less electrons flowing out of n-GaAs, because the electrons recombine at p-GaAs.

If we grow the p-$Ga_{1-x}Al_xAs$ layer on p-GaAs, the electrons recombination at p-GaAs is lower than 10^4 cm/s. and p-$Ga_{1-x}Al_xAs$ generates ΔE_C to reflect more electrons flowing to n-GaAs. Then the efficiency is high.

Energy band gap of $Ga_{1-x}Al_xAs$ depends on the content of Al, if x=0.7 the energy gap is 2.5eV. It is suitable for wavelength of photons of solar spectrum. So if we increase thickness about 10μm, the sheet resistance of $Ga_{1-x}Al_xAs$ is decreased.

Heterojunction solar cells consist of n and p type semiconductor. P or n type has wide band gap semiconductor on the top. The photon with energy less than band gap of top layer can pass through, so called this layer as " window layer " and this phenomena is called " window effect ".

The photon can pass through the window layer, and then is absorbed at the next layer which has lower energy band gap generates electron and hole pair. The heterostructure solar cells have high spectral response with photon energy in between

ศูนย์วิทยทรัพยากร
จุฬาลงกรณ์มหาวิทยาลัย

band gap energy of both semiconductors. We can reduce the sheet resistance of solar cells by growing thick window layer and this window can protect other radiation in space.

Hence, to design heterojunction solar cells, they have to select approximate band gaps of both semiconductors material relate to the spectral response of sunlight.

On the **table 2.1** shows the lattice mismatch and band discontinuity of semiconductor pair formed heterojunction. The definition of lattice match is the difference of lattice constant of two type semiconductors contacted **[12]**.

Table 2.1 Lattice mismatches and band discontinuity of semiconductor that we make the heterojunction anisotype.

Semiconductors	**Lattice mismatch (%)**	**Band discontinuity**
p-$Ga_{0.4}Al_{0.6}As$/n-GaAs	0.08	$\Delta E_v \approx 0$ eV
n-CdS/p-InP	0.9	$\Delta E_c \approx 0.12$ eV
n-CdS/p-CdTe	9.7	$\Delta E_c \approx 0.22$ eV
n-CdS/p-Cu_2S	4.6	$\Delta E_c \approx 0.2$ eV

ศูนย์วิทยทรัพยากร
จุฬาลงกรณ์มหาวิทยาลัย

CHAPTER III
RESEARCH METHODOLOGY

3.1 General

Upon completion of this master's degree project, thorough planning and scheduling have been organized on the methodology and research sequence to ensure a smooth running of the research program from literature review, experimental data collection, discussion and validation of result and conclusion.

3.2 Literature Review

Literature review involves a thorough search and investigation of solar cells related issues through many different sources such as text books, articles, journals, international conference papers. Additionally, there is also searching and browsing through internet web pages, internet websites, online library, online articles and journals to seek complementary information. The aim of literature review is to gather important information related to the topic and to deepen the proper understanding of the knowledge and competencies of heterojunction solar cells characterization.

3.3 Experimental Data Correction

Not only literature review on the solar cell basic theory but also the experimental study on heterojunction solar cells is needed to gain practical information.

The technologies and equipment utilized to gather the useful practical information are Liquid Phase Epitaxy (LPE), Molecular Beam Epitaxy (MBE), Photoluminescence Measurement, Vacuum Evaporation, I-V curve Measurement, and Spectral Response Measurement Machine, etc. The description of LPE and MBE technologies, and also photoluminescence will be provided.

3.3.1 Liquid Phase Epitaxy (LPE)

Since its invention by Nelson in 1963 **[13]** Liquid Phase Epitaxy (LPE) has proved to be a versatile, flexible method to grow thin layer of III-V, II-VI and IV-VI compound for material investigations and device application. Many”first” of electronic devices were based on LPE structure. One important example was the GaAs/AlGaAs double-heterostructure (DH) laser diode continuous-wave (CW) lasing at the room temperature **[14, 15]**. The LPE technique has many advantages, there are

Figure 3.1 Horizontal LPE systems **[16]**

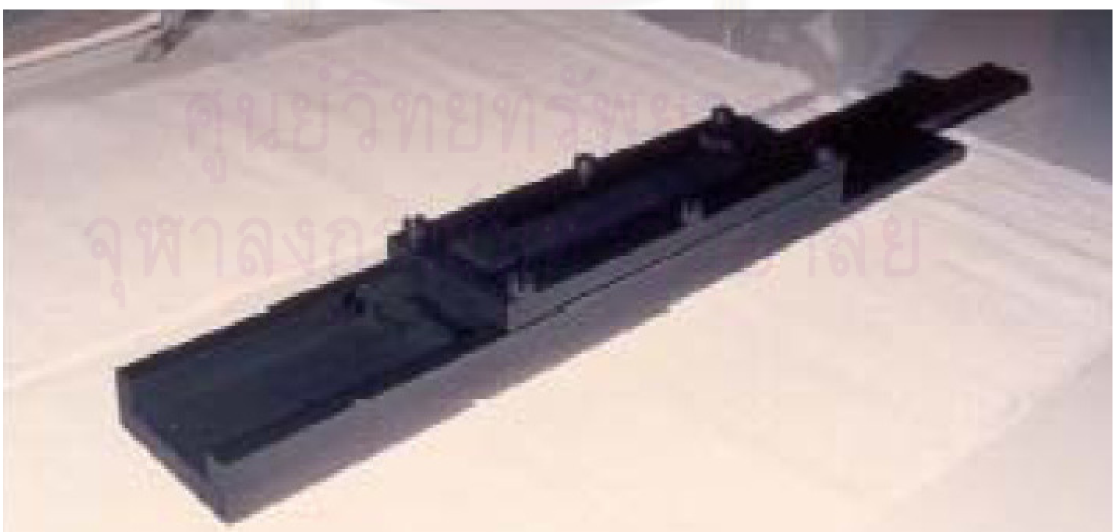

Figure 3.2 Multi-bin graphite boats **[16]**

(1) Experimental setup is simple and inexpensive.

(2) Growth temperature is low (approximately 350 to 900°C).

(3) Relatively height growth rate of 0.1 mm/min is possible.

(4) Elimination of hazards due to use of reactive gasses and their reactive products.

(5) Non-requirement of vacuum equipment.

The limitations of LPE technique is the difficulty of growing layers that differ in lattice constant by more than ~1% from substrate and its inability to produce ultra-thin layer whose thickness is less than 0.1µm. Furthermore, LPE layers generally do not have a good surface morphology as layers grown by Vapor Phase Epitaxy (VPE), as well as Molecular Beam Epitaxy (MBE). However, because of simplicity and flexibility, LPE has been attractive for growing complex layered structure required for optoelectronic devices.

The horizontal LPE system, which is installed at Chulalongkorn University, Semiconductor Device Research Laboratory (SDRL) is shown on **figure 3.1.** The apparatuses use for LPE systems are

(1) Programmable temperature controller.

(2) Movable resistance furnace.

(3) Quartz tube.

(4) Pd-purified H_2 as well as gas system.

(5) Hygrometer.

(6) Nitrogen hood.

(7) Thermocouple as well as gas system.

(8) Multi-bin graphite boat (see on **figure 3.2**).

(9) Quartz rode (use for sliding).

Actually, LPE is suitable for growing thick epitaxial layers quickly because the growth rate is high and it is also suitable for forming multi-layers structures, such as heterostructures because it has multi-bins graphite boats **[16]**.

3.3.2 Molecular Beam Epitaxy (MBE)

Molecular beam epitaxy (MBE) is a process for growing thin, epitaxial films of a wide variety of materials, ranging from oxides to semiconductors to metals. It was first applied to the growth of compound semiconductors. That is still the most common usage, in large part because of the high technological value of such materials to the electronics industry. In this process beams of atoms or molecules in an ultra-high vacuum environment are incident upon a heated crystal that has previously been processed to produce a nearly atomically clean surface. The arriving constituent atoms form a crystalline layer in registry with the substrate, i.e., an epitaxial film. These films are remarkable because the composition can be rapidly changed, producing crystalline interfaces that are almost atomically abrupt. Thus, it has been possible to produce a large range of unique structures, including quantum well devices, superlattices, lasers, etc., all of which benefit from the precise control of composition during growth. Because of the cleanliness of the growth environment and because of the precise control over composition, MBE structures closely approximate the idealized models used in solid state theory **[17]**.

3.3.2.1 The MBE system

The Molecular Beam Epitaxy (MBE) is consisting of four chambers: load chamber, introduction chamber, transfer chamber, and growth chamber. Each

ศูนย์วิทยทรัพยากร
จุฬาลงกรณ์มหาวิทยาลัย

chamber is separated by isolated gate valves and the substrate is transferred from load chamber to each other chamber. The introduction and growth chambers are heater for a heat the substrate. The ultra-high vacuum is obtained via the pumping systems are consisting of sorption pump, ion pump, titanium sublimation pump.

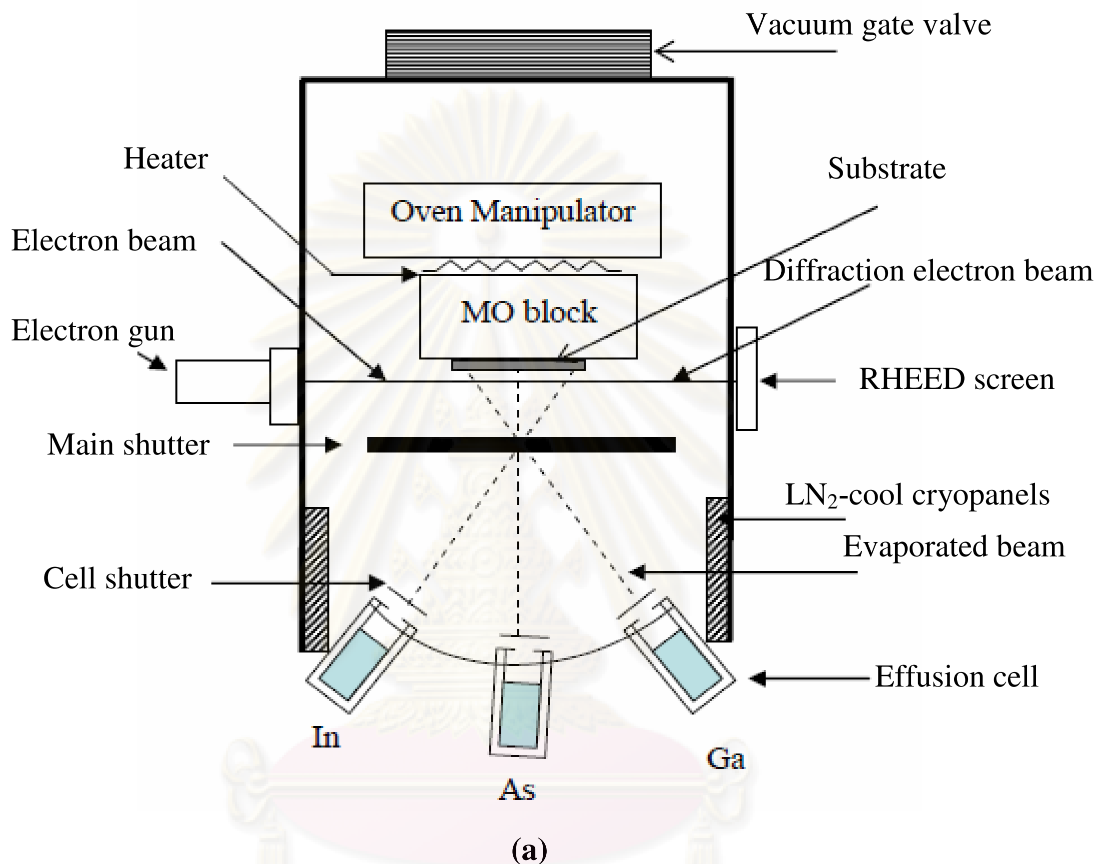

(a)

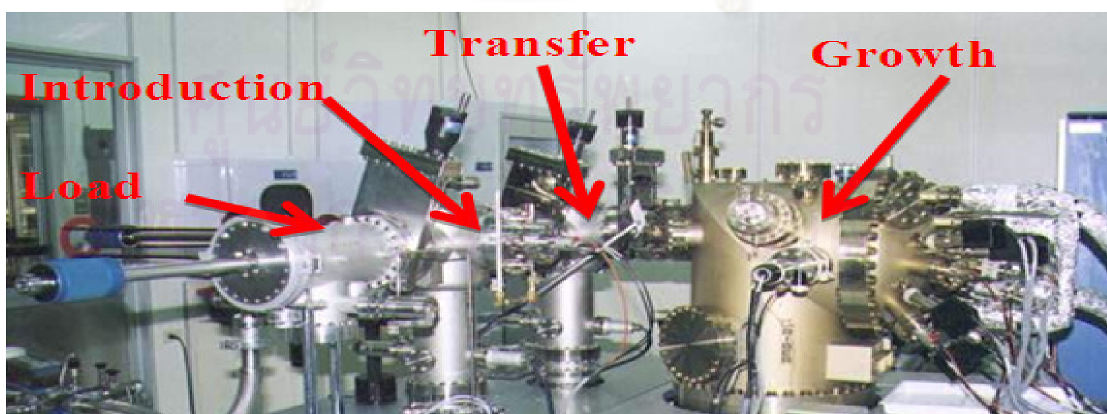

(b)

Figure 3.3 **(a)** diagram of growth chamber and **(b)** schematic illustration of a RIBER 32P MBE system **[16]**

The diagram of a typical MBE growth chamber shows in **figure 3.3 (a)**. Inside the growth chamber of the MBE are material source cells, substrate heater, monitoring equipment, and pumping system. The solid source of materials is separately contained different effusion cells. During the MBE working, the chamber wall and effusion cells are cooling by liquid N_2 to protect contamination as result of outgases from heated part. There are two type of monitoring equipments such as mass spectroscopy and reflection high-energy electron diffraction (RHEED). The mass spectroscopy is used for particle analysis, and RHEED is used to observe the surface of crystallization during the MBE grows. And there are two ionization gauges which measures the beam flux and background pressure (BP). And one of the ionization gauges is measured for BEP is located at the level of manipulator behind the substrate, and the other gate is situated in front of ion pump for measuring background pressure. The temperature measures by W-Re thermocouple and the temperature is controlled by computer via a controller card (EUROTHERM). In order to get a uniforms flux profile on the surface of the substrate during epitaxy. All of the samples are grown on semi-insulating (001)-GaAs substrates in the solid source MBE system (RIBER 32P) shows in **figure 3.3(b)**. The substrate is attached to molybdenum block (MO in the figure). The prior to crystal growth, the contamination is removed from substrate surface for 3 hour pre-heat process in the introduction chamber before being transferred to the growth chamber. The pre-heat process has done when the pressure in the introduction chamber is $1X10^{-8}$ Torr or lower than. The temperature profile of pre-heat process shows on the **figure 3.4**.

ศูนย์วิทยทรัพยากร
จุฬาลงกรณ์มหาวิทยาลัย

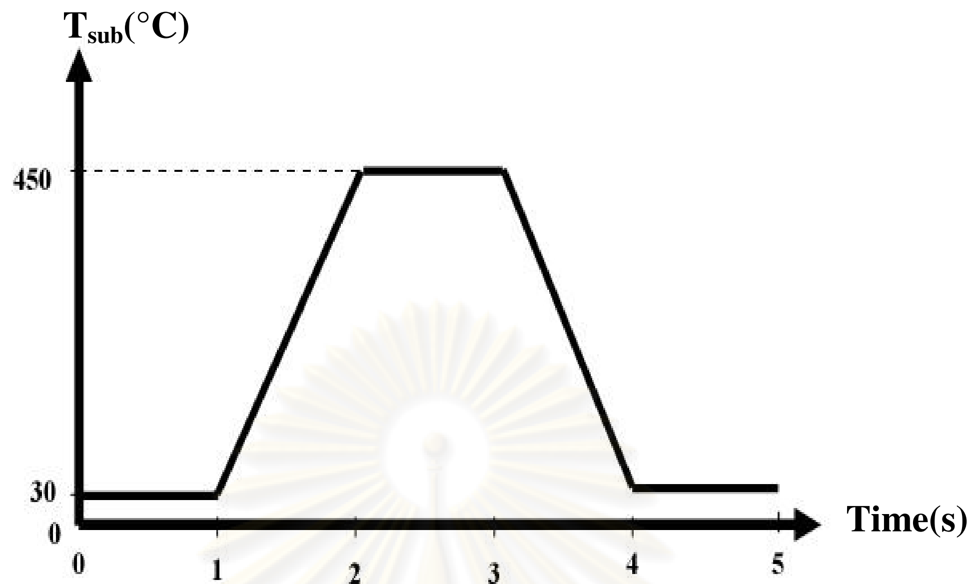

Figure 3.4 Temperature profile of the pre-heat process **[17].**

In the pre-heat process, the sample is heat by increasing the temperature of the substrate (T_{sub}) from 30°C to 450°C at the rate of 7°C/min, to take one hour for ramp up. During ramp up, the contaminations from the substrate surface is removed and purges, at that time the pressure also increases. Then the T_{sub} is ramp down from 450°C to 30°C. The pre-heat process, this takes three hours and almost of the samples are subject to this process without exception.

When we finish pre-heat process, the substrate is transferred to growth chamber and de-gas is carrier out. The temperatures of effusion cells are increased from standby temperature (T_{std}) to require temperature in order to remove contaminations from each effusion cells. The profile of de-gas process for the temperature is ramp up for Ga and In effusion cells are shown on the **figure 3.5**, and As effusion cell and substrate are shown on the **figure 3.6**.

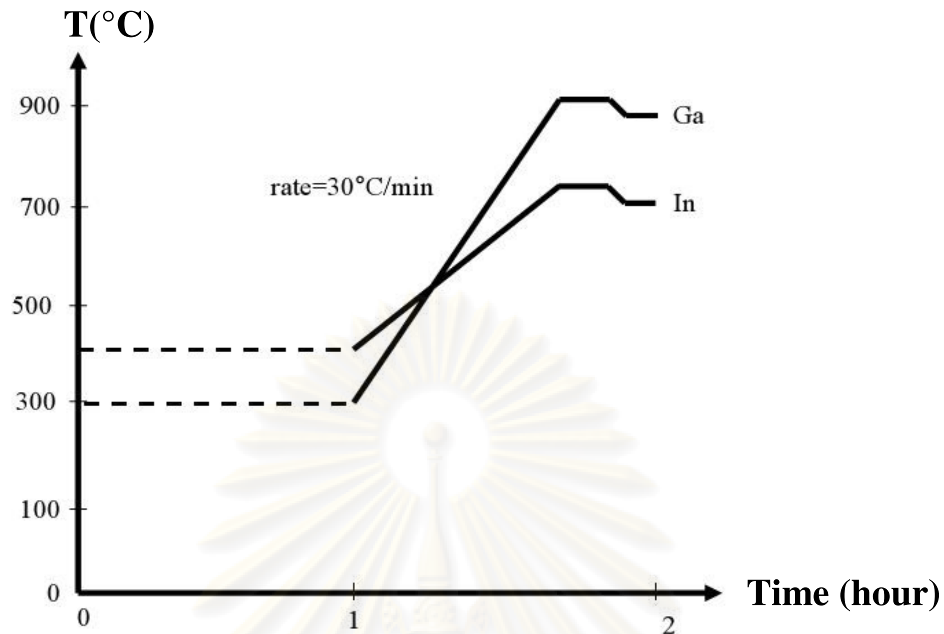

Figure 3.5 Temperature of Ga and In effusion cells. The effusion cell is closed in the dotted line range and opened in solid line range during respective temperature ranges **[17]**.

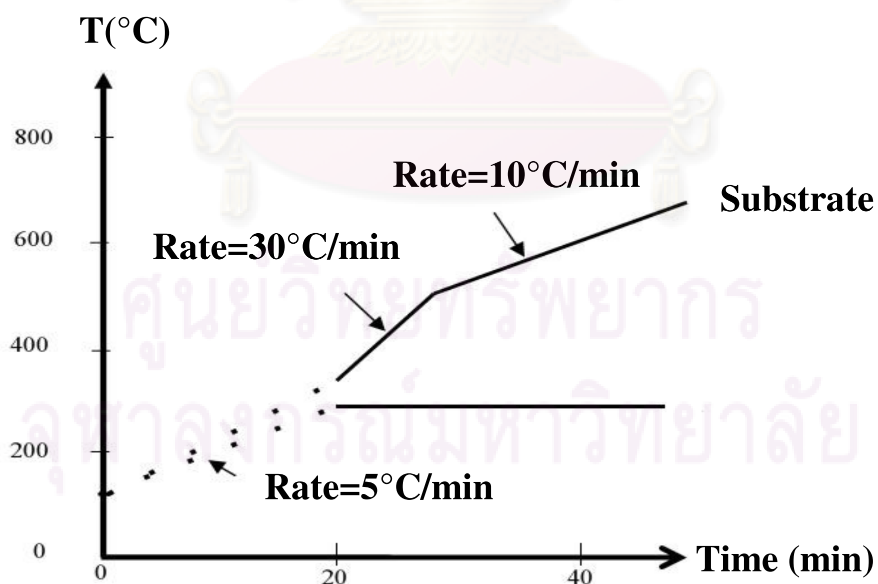

Figure 3.6 Temperature profile of As effusion cell and substrate. The effusion is closed in the dotted line range and opened in solid line range during respective temperature ranges **[17]**.

The **figure 3.5**, the temperatures of Ga and In effusion cells are increased from their standby temperature (T_{std}) to the set point temperature at the same rate of 30°C/min. After ramp up the temperature of the effusion cell, then the each effusion cell is measured by opening corresponding cell. Typically, BEP of In, Ga and As effusion cells are ~10^{-8}, 10^{-7} and 10^{-6} Torr respectively. The de-gas process of effusion cell has done last because the BEP of As effusion cell is significantly higher than other effusion cells. So the temperature of the de-gas of As effusion cell and substrate are ramp up in he same time from T_{std} 100°C to 300°C in the same rate of 5°C/min in order to suppress the As atoms out gassing from the substrate surface. When the T_{sub} increases higher than 300°C, out gassing As atoms from the substrate result in the surface roughness. Between 300°C to 500°C, rate of 30°C/min. Between 500°C to 650°C, the rate of 10°C/min. After de-gas process which prepares the effusion cells for growing, then the substrate has to de-oxide process in order to prepare the surface for subsequent epilayer growth. The de-oxide process and RHEED pattern for substrate, the temperature increases in this process is shown in **figure 3.7(a)**. When T_{sub} is arrived 580°C, the spotty pattern shows in **figure 3.7(b)** start to occur because the native oxide goes out from the GaAs substrate. To ensure complete oxide removal and thus a clean GaAs surface, the temperature is kept at slightly above the de-oxide temperature. Usually, T_{deox}=580°C, the temperature would be kept at 590°C until the CO peak is almost flat.

ศูนย์วิทยทรัพยากร
จุฬาลงกรณ์มหาวิทยาลัย

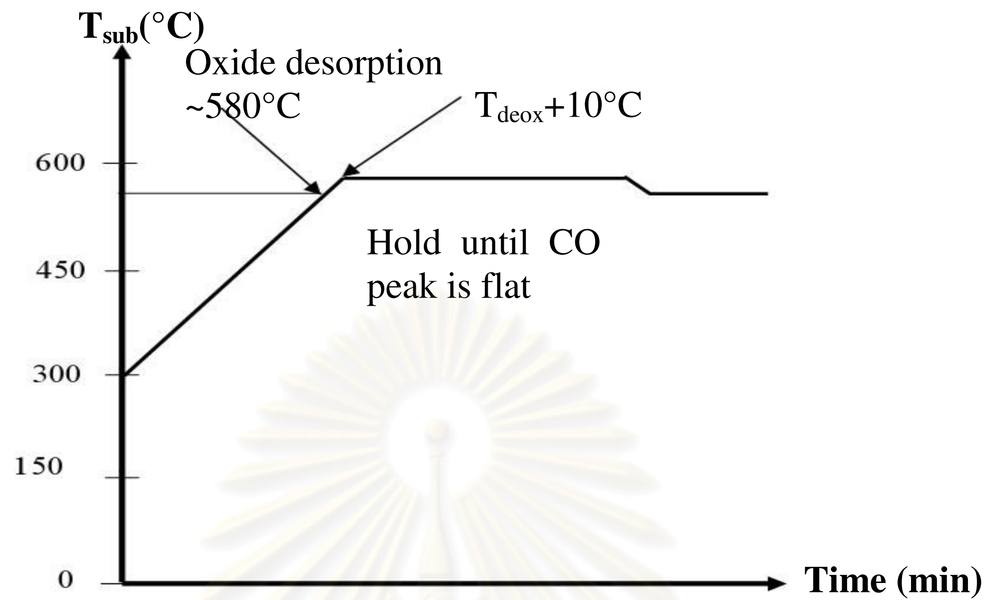

(a)

(b)

Figure 3.7 **(a)** temperature profile of the oxide desorption process and RHEED pattern when the temperature increases and **(b)** photo took from view port showing RHEED spotty pattern at de-oxide temperature at 580°C **[17]**

3.3.2.2 In-situ characterization tools

There are two important in-situ characterization tools such as mass spectroscopy and RHEED. The mass spectroscopy is used to investigate the chemical constitutes inside the growth chamber. And the RHEED is used to calibrate the growth rate and indicate the 2D and 3D growth mode transition point.

★ **Mass Spectroscopy (An introduction to Mass Spectroscopy, Ashcroft)**

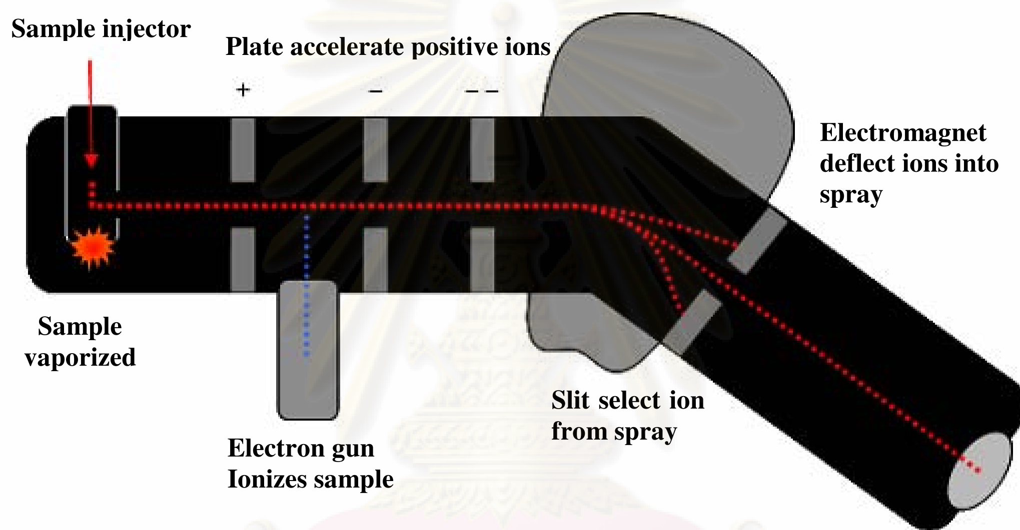

Figure 3.8 Schematic diagram of mass spectrometer
(From: www.stev.gb.com/science/spectroscopy.html)

The mass spectroscopy is an analytical technique uses to measure mass-to-charge (m/z) ratio of ions. The composition of a sample is determined from the mass spectrum representing the masses. A typical mass spectrometer is comprised three parts such as ion source, a mass analyzer, and detector system. The **figure3.8** is shown the schematic diagram of spectrometer. The sample is introduced into ionization source of the instrument. Inside the ionization source, the sample molecules are ionized, because ion is easier to manipulate than neutral molecules. These ions are extracted into analyzer region of mass spectrometer where they separate according to

their mass-to-charge ratios. The separated ions have been detected and this signal is sent to a data system where the m/z ratios to store together with their relative abundance for presentation in the format of m/z spectrum. In experiment, masses of particle such as hydrogen, helium, argon, water, oxygen, carbon dioxide, and monoxide have been checked by mass spectrometer. Especially, the complete removal of native oxide from the substrate surface is investigated by mass spectrometer. In de-oxide process, when the signal 28 peak (carbon monoxide) is flat, further growth process is continued.

★ **Reflection High-Energy Electron Diffraction (RHEED)**

Undoubtedly the single most important analytical tool for layer grower has been the RHEED system for real time observation of the crystal structure of the growth. Most MBE systems today either include an electron gun and phosphor screen for displaying RHEED pattern while the layer is growing, the photo of the film pattern is shown on **figure 3.7 (b) [16]**. And the RHEED system provides a tool for monitoring growth rate, for a qualitative measure of surface topography and for monitoring surface structure that, in certain instances, can provide a measure of the surface composition. Also important to the user is that the RHEED system is relatively insensitive to the ambient in the growth chamber, that is, RHEED images can be obtained with equal clarity either while beams are incident on the substrate or when the growth has been terminated and the substrate is cooled; furthermore the geometry is such that there is no part of the RHEED system positioned in front of the sample to block access to the surface since the RHEED arrives at a glancing angle **[19].** The **figure 3.9** is shown the schematic diagram presentation of RHEED geometry shows the incident electron beam at an angle Θ to the surface plane.

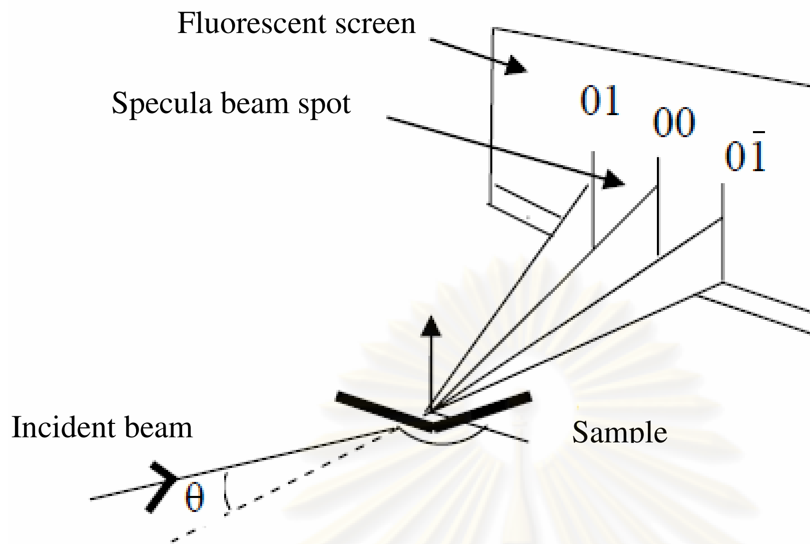

Figure 3.9 Schematic diagram presentation of RHEED geometry shows incident electron beam at an angle Θ to the surface plane **[18].**

3.3.3 Photoluminescence (PL)

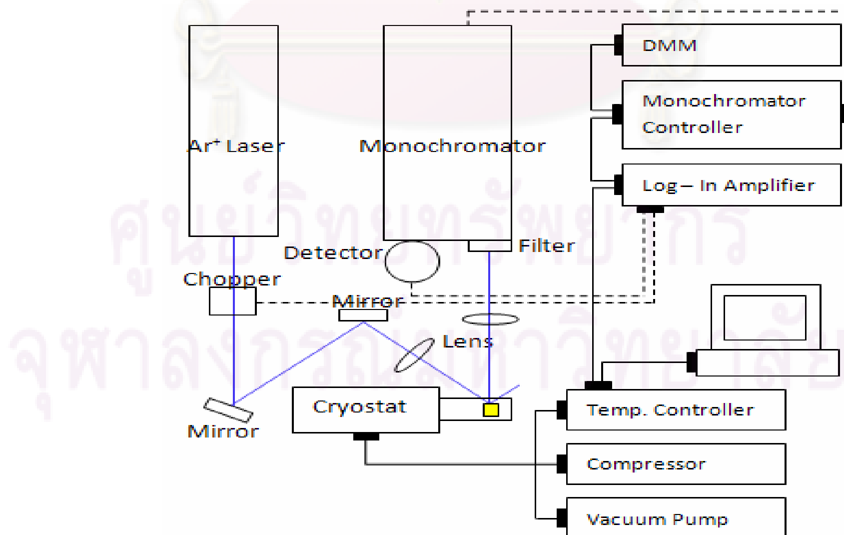

Figure 3.10 Schematic diagram of PL experiment set up.

The photoluminescence is a light emission properties of semiconductor when excited by photon energy. While the semiconductor is excited, electron-hole pair is generated and recombined. The resulting radiation from the recombination of carriers is called Photoluminescence (PL) **[19].**

The photoluminescence (PL) spectroscopy is a useful technique for the study and characterization of material and dynamical processes occurring in materials. However, PL spectroscopy, like all other experimental technique, does not give a universal, all-encompassing view of energy aspect of the properties of a particular material, or even more specifically of the optical properties of materials.

Photoluminescence from semiconductor is most commonly characterized via spectroscopic techniques. These techniques involve measuring the energy distribution of emitted photons after optical excitation. This energy distribution is then analyzed in order to determine properties of the material, including defect species, defect concentration, possible stimulated emission, etc. This technique for material characterization has achieved significant success and popularity in this regard at least party due to the simplicity of the technique and absence of sample process requirements **[20]**.

3.4 GaAs and AlGaAs for LPE

The GaAs and AlGaAs are the basic materials for solar cell structure. The understanding of these materials preparation and weight calculation are very important and will be provided by this section.

3.4.1 Material preparation

The material which it can be used to fabricate GaAs or $Al_xGa_{1-x}As$ epilayer should be commonly prepared in the Ga solvent and as other materials such as As, and dopant is also prepared as solute. The commonly n-type dopant is Sn or Te, and for the p-type dopant is Ge or Zn. These materials are prepared in solid form and can calculate by the formula below.

$$X_{Ga} + X_{As} + X_{Al} + X_{im} = 1 \quad \textbf{(3.1)}$$

X is the m ole fraction of each other element in $Al_xGa_{1-x}As$ alloy. The Ga weight (W_{Ga}) to As weight (W_{As}) can be writing as

$$W_{As} = (X_{As} / X_{Ga})(M_{Al} / M_{Ga})W_{Ga} \quad \textbf{(3.2)}$$

M is the atomic weight of each element. Then other element can be writing

$$W_{Al} = (X_{Al} / X_{Ga})(M_{As} / M_{Ga})W_{Ga} \quad \textbf{(3.3)}$$

$$W_{im} = (X_{im} / X_{Ga})(M_{im} / M_{Ga})W_{Ga} \quad \textbf{(3.4)}$$

The weight of GaAs is given by

$$W_{GaAs} = (X_{GaAs} / X_{Ga})(M_{GaAs} / M_{Ga})W_{Ga} \quad \textbf{(3.5)}$$

Where M_{Ga}=69.72 M_{As}=74.92

M_{Al}=26.98 M_{Ge}=72.59

M_{Sn}=118.69 M_{Te}=127.60

M_{GaAs}=M_{Ga}+M_{As}=144.64

The value of each element can be approximated from graphs as shown in **figure 3.11, 3.12, 3.13 and 3.14**

ศูนย์วิทยทรัพยากร
จุฬาลงกรณ์มหาวิทยาลัย

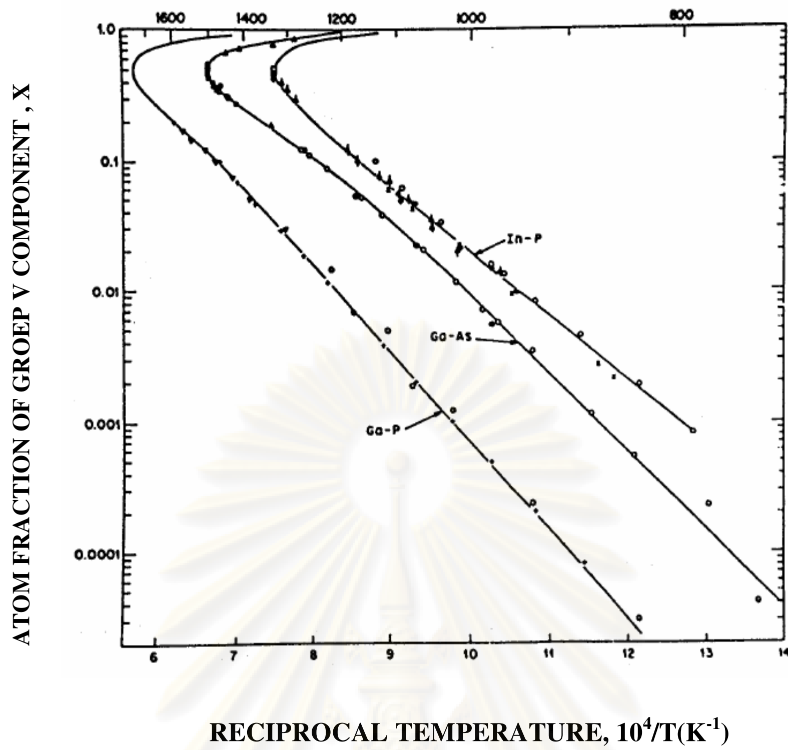

Figure 3.11 Liquidus composition versus reciprocal temperature for GaAs, GaP and InP **[21]**.

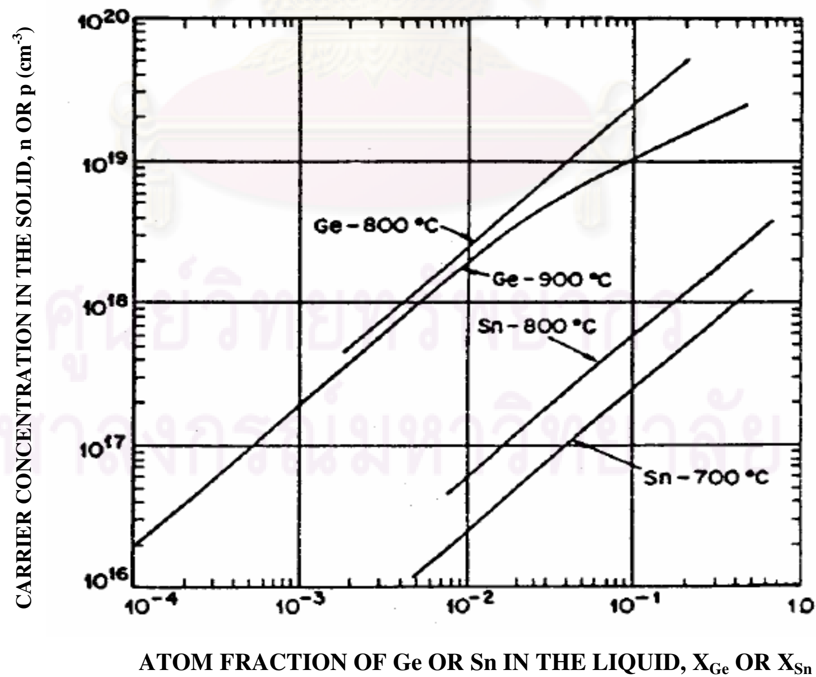

Figure 3.12 Room temperature hole concentration in GaAs versus the atom fraction of Ge in the liquid along the 800 and 900°C and the lower curves are the

ศูนย์วิทยทรัพยากร
จุฬาลงกรณ์มหาวิทยาลัย

room temperature electron concentration in GaAs versus the atom fraction of Sn in the liquid along the 700 and 800°C **[21]**.

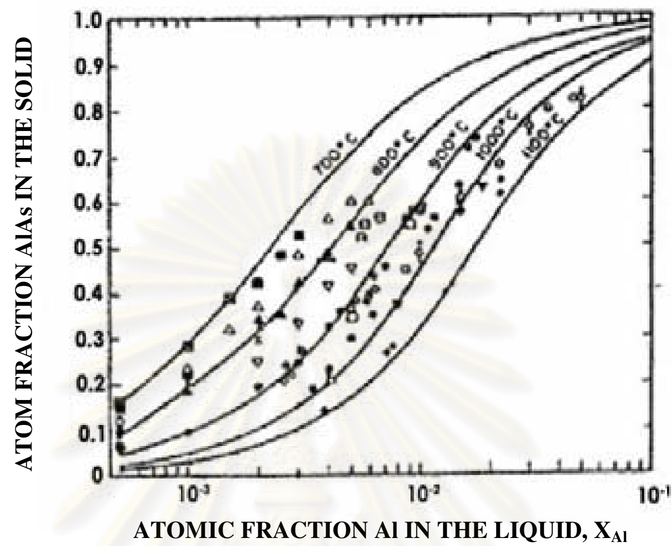

Figure 3.13 Solidus compositions in $Al_xGa_{1-x}As$ as a function of liquidus composition **[21]**.

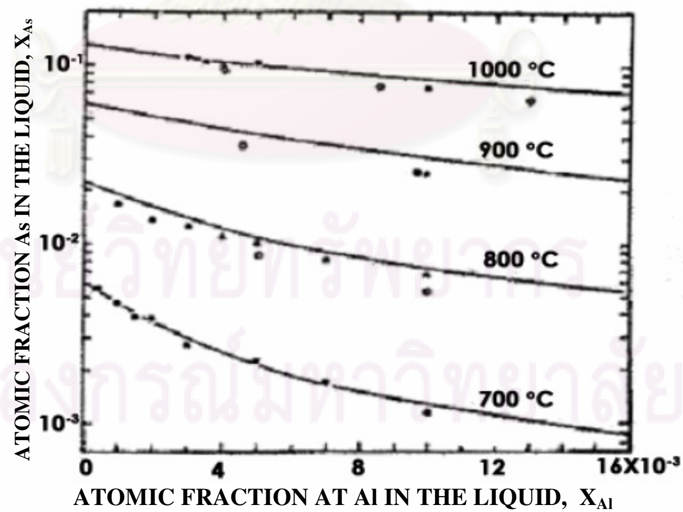

Figure 3.14 Liquidus isotherms in the AlGaAs system **[21]**.

ศูนย์วิทยทรัพยากร
จุฬาลงกรณ์มหาวิทยาลัย

3.4.2 Material weight calculation

The weight of materials are calculated by the following

- **$Al_{0.35}Ga_{0.65}As$ (p) $10^{18}cm^{-3}$, Ge-doped**

$X_{Al}=0.0025$

$X_{Ge}=0.04$

$X_{As}=0.015$

Then $X_{Ga}=1-X_{Al}-X_{As}-X_{Ge}=0.9425$

We use 3g of Ga, therefore we get

$W_{Al} = (X_{Al}/X_{Ga}).(M_{Al}/M_{Ga}).W_{Ga}$

$= (0.0025/0.9425).(26.98/69.72).3g$

$= 3.079mg$

$W_{GaAs}= (X_{GaAs}/X_{Ga}).(M_{GaAs}/M_{Ga}).W_{Ga}$

$\approx (X_{As}/X_{Ga}).(M_{GaAs}/M_{Ga}).W_{Ga}$

$= (0.015/0.9425).(144.64/69.72).3g$

$= 99.05mg$

$W_{Ge}= (X_{Ge}/X_{Ga}).(M_{Ge}/M_{Ga}).W_{Ga}$

$= (0.04/0.9425).(72.59/69.72).3g$

$= 120mg$

- **$Al_{0.35}Ga_{0.65}As$ (p^+) $5x10^{18}cm^{-3}$, Ge-doped**

$X_{Ge}=0.025$

$X_{Al}=0.0025$

$X_{As}=0.015$

Then we get $X_{Ga}=1-X_{Al}-X_{As}-X_{Ge}=0.97$

We use 3g of Ga, therefore we get

$W_{Al} = (X_{Al}/X_{Ga}).(M_{Al}/M_{Ga}).W_{Ga}$

$= (0.0025/0.97).(26.98/69.72).3g$

$= 3mg$

$W_{GaAs}= (X_{GaAs}/X_{Ga}).(M_{GaAs}/M_{Ga}).W_{Ga}$

$\approx (X_{As}/X_{Ga}).(M_{GaAs}/M_{Ga}).W_{Ga}$

$= (0.0015/0.97).(144.64/69.72).3g$

$=96.66mg$

$W_{Ge}= (X_{Ge}/X_{Ga}).(M_{Ge}/M_{Ga}).W_{Ga}$

$= (0.025/0.97).(72.59/69.72).3g$

$= 80.70mg$

- **GaAs (n^-)**

$X_{As}=0.022$

Then we get $X_{Ga}=1-X_{As}=0.978$

We use 3g of Ga, therefore we get

$W_{GaAs}= (X_{GaAs}/X_{Ga}).(M_{GaAs}/M_{Ga}).W_{Ga}$

$\approx (X_{As}/X_{Ga}).(M_{GaAs}/M_{Ga}).W_{Ga}$

$= (0.022/0.978).(144.64/69.72).3g$

$= 140.01mg$

- **GaAs (p^+) $5x10^{18}$ m^{-3}**

$X_{As}=0.022$

$X_{Ge}=0.02$

Then we get $X_{Ga}=1-X_{As}-X_{Ge}$

$= 1-0.022-0.02$

$= 0.96$

$W_{GaAs}= (X_{GaAs}/X_{Ga}).(M_{GaAs}/M_{Ga}).W_{Ga}$

$\approx (X_{As}/X_{Ga}).(M_{GaAs}/M_{Ga}).W_{Ga}$

$= (0.022/0.96).(144.64/69.72).3g$

$= 142.2mg$

$W_{Ge} = (X_{Ge}/X_{Ga}).(M_{Ge}/M_{Ga}).W_{Ga}$

$= (0.02/0.958).(72.59/69.72).3g$

$=60mg$

Table 3.1 Material weight

Material / Solution	Ga(g)	GaAs(mg)	Al(mg)	Ge(mg)
$Al_{0.35}Ga_{0.65}As(p^+)$	3	96.66	3	80.70
$Al_{0.35}Ga_{0.65}As(p)$	3	99.05	3.079	120
$GaAs(p^+)$	3	142.2	-	60
$GaAs(n^-)$	3	140.01	-	-

3.5 Growth process

3.5.1 Liquid phase epitaxy

The growth process is run after the boat is loaded with substrate and the material solution is already preparation, and it is placed in the quartz tube, but initially remains outside the furnace. First, it is flushed with flowing N_2, evaluated and checked for leaks about 1 hour, and then flowing Pd-purified H_2 (prevents oxidation of solution and substrate). The furnace is moved into the position for heating the boat **figure 3.15 (a)** shows the basic set up of LPE system**, figure 3.15 (b)** and **(c)** illustrate schematic profile of the furnace temperature versus the growing time duration, samples **G** and **H**.

ศูนย์วิทยทรัพยากร
จุฬาลงกรณ์มหาวิทยาลัย

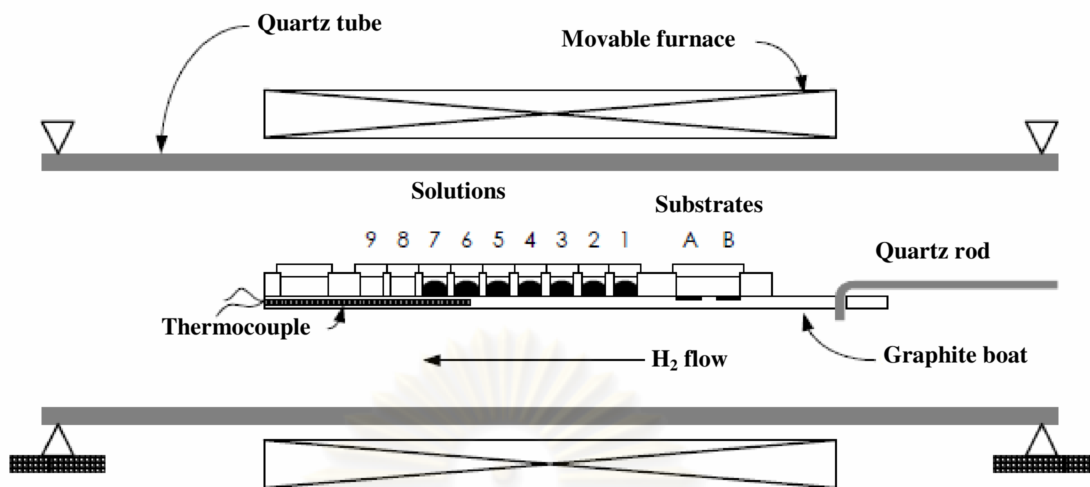

(a)

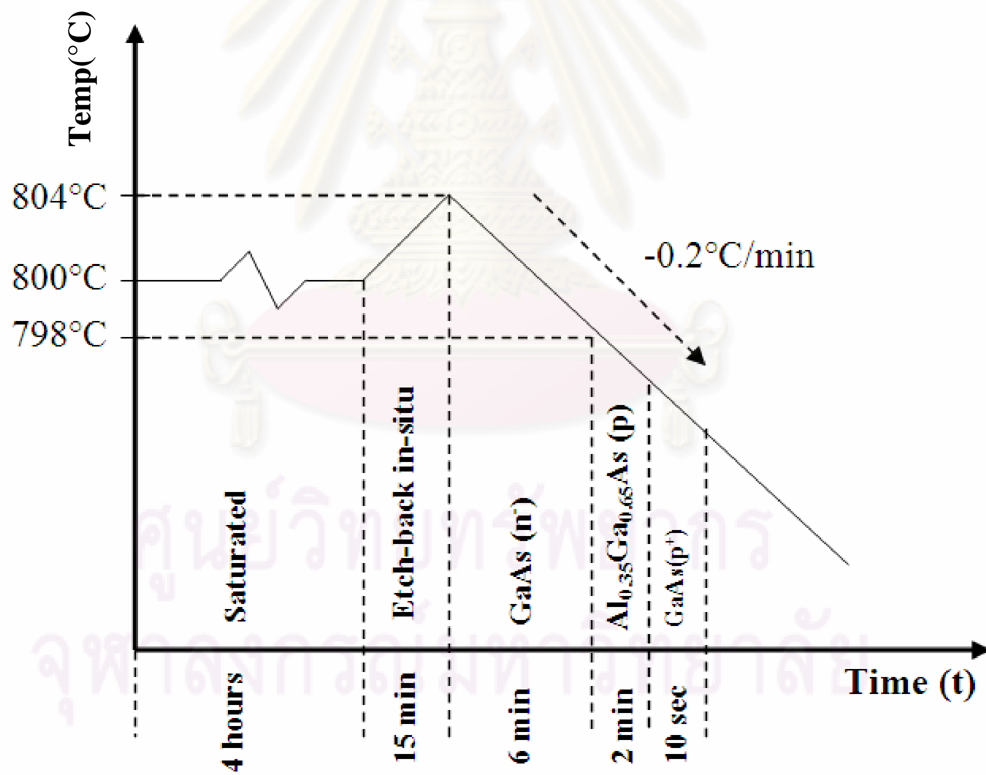

(b)

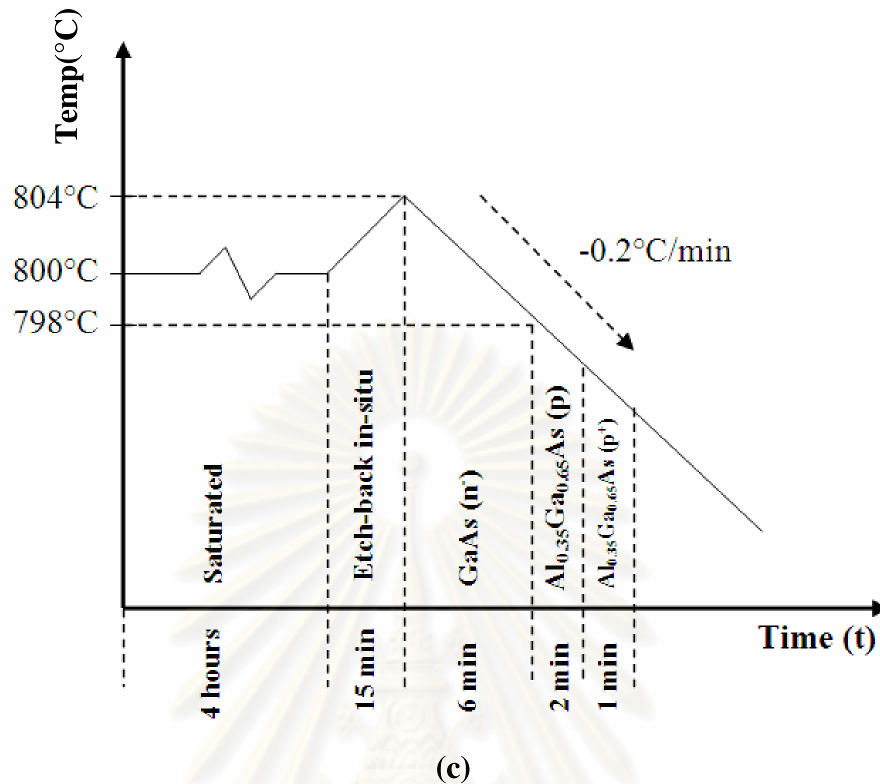

(c)

Figure 3.15 **(a)** Basic set up of LPE system, **(b)** and **(c)** schematic profile of the furnace temperature versus the growing time duration, samples **G** and **H**.

The temperature is kept constant at 800°C at least for 4 hours to substrate, material and solution, then step up to 804°C for in-situ etching. When the temperature reaches peak of 804°C, and then it decreases at the rate of 0.2°C/min to saturate the material solution, then the temperature of the solution is below the saturation condition, and the epitaxial layer started growth. In the other hand, the temperature is more decreasing, the solution is oversaturated, then the oversaturated comes into contact with the substrate, the oversaturated temperature, ΔT will, therefore, force the solution GaAs to precipitate. The growth layer is terminated by sliding the substrate out from under solution. The thickness of growth layer can be determined by the oversaturated temperature and the range of time which the substrate and solution are contact and can calculate by equation of **3.6**.

$$d = K\left(\Delta T^{\frac{1}{2}} + \frac{2}{3}\alpha t^{\frac{3}{2}}\right) \qquad \textbf{(3.6)}$$

K : The constant which is a function concentration of As in the liquid

ΔT : The over saturation temperature of solution

α : The cooling rate

3.5.2 Molecular Beam Epitaxy

The growth process of MBE briefly discusses below

- The GaAs substrate (100) is loaded into the MBE, and is cleaned by chemical; it is the case that the substrate is epi-ready type and kept in a dust-free condition. After mounting on the molybdenum block with indium, the substrate is preheated at 450°C for one hour in the preparation chamber, then the substrate transferred to the growth chamber, this chamber is cooling by liquid nitrogen, and the titanium sublimator of the growth chamber is switched off.

- Increase the substrate temperature (OM= oven manipulator) as well as the Al, Ga and Si containing cell.

OM 100°C ⟶ 250°C

Al 300°C ⟶ Calibrate from the flux pressure

Ga 300°C ⟶ 910°C

Si 300°C ⟶ depend on the carrier concentration

- Rotate the manipulator up of 224 degree to obtain the "optimum" flux pressure measurement position. First, the Ga flux will be measured. The Ga containing cell and the main shutter are then opened, while the other shutter is closed. Adjust the Ga cell temperature to get the flux pressure of 4.3×10^{-7}Torr (wait until the pressure is stabilized). The growth rate of GaAs is gotten 0.8μm/hour. Close the individual cell shutter as well as the main shutter. To get the ternary compound $Al_{0.1}Ga_{0.9}As$, we have to adjust the Al cell temperature by reading on the gauge.

$$\text{Al flux} = (\text{Ga flux}) \times \frac{10}{90} \text{ (mole fraction)} \times \frac{0.92}{1.68} \text{ (gauge sensitivity)}$$

$$= 2.6164 \times 10^{-8} \text{Torr}$$

And the $Al_{0.2}Ga_{0.8}As$, $Al_{0.3}Ga_{0.7}As$

★ $Al_{0.2}Ga_{0.8}As$

$$\text{Al flux} = 4.3 \times 10^{-7} \times \frac{20}{80} \times \frac{0.92}{1.68}$$

$$= 5.8869 \times 10^{-8} \text{Torr}$$

★ $Al_{0.3}Ga_{0.7}As$

$$\text{Al flux} = 4.3 \times 10^{-7} \times \frac{30}{70} \times \frac{0.92}{1.68}$$

$$= 1.0092 \times 10^{-7} \text{Torr}$$

Gradually increase the As cell temperature up to 190°C. To make small steps (5°C/min each). The individual shutter of the As containing cell is opened, as well as the main shutter. All other individual shutters are closed. The partial pressure of As_4 is about 20 times grater than Ga, so it might reach about 8.6×10^{-6}Torr. During the time, the substrate temperature is adjusted to be 300°C.

● Rotate up the manipulator to obtain 320 degree (still remain opened the main shutter as well as As cell). Increase the substrate temperature to 550°C. The electron gun of RHEED system is powered on and the shutter that protects the RHEED screen is opened. By using the deflectors, position the electron beam so that it strike the substrate. A diffused light must be observed on the screen, and possibly circles due to the surface oxide. Gradually increase the substrate temperature (10°C each step) until spotty pattern is clearly observed. To set the substrate temperature cools down by 20°C less than that of the temperature. Deoxidation is processed for approximately 10-15 minutes. The streaky pattern will slowly appear. They gradually become less and less diffuse as the oxide evaporates.

- Open the Ga individual shutter to begin the GaAs deposited on the substrate. To store at this condition until the designed thickness (2 minutes and 30 second to obtain 2μm of GaAs epitaxy for the growth rate 8.8μm/hour). Other cell shutter such as Al and Si are also opened if either the AlGaAs epitaxial layer or dopant is required **[21].**

ศูนย์วิทยทรัพยากร
จุฬาลงกรณ์มหาวิทยาลัย

CHAPTER IV
EXPERIMENTAL RESULT AND DISCUSSION

4.1 General

This chapter is composed of all the experimental results and discussions of research data. The samples are grown by Liquid Phase Epitaxy (LPE) and Molecular Beam Epitaxy (MBE). There are three kinds of AlGaAs/GaAs heterostructure solar cells. The first one is of Schottky barrier diode, the second one is of fixed Al content window layer and the third one has Al content of 0.3, 0.2, and 0.1 window layer. All of them were separately analyzed for spectral response, photoluminescence, and I-V curve measurements. Some of them are calculated for their fill factors and efficiencies. Basically, the analysis is divided into two categories in this study. First group of samples are grown by MBE and the second group of samples are grown by LPE. These two growth techniques are compared in terms of their solar cell structures and performances.

4.2 Heterostructure Solar cells realization

There are six samples fabricated by MBE and two samples by LPE. Their solar cell structures are shown in **figure 4.1~4.6**. The samples **A, B, C, D, E** and **F** are fabricated by MBE, and samples **G** and **H** are fabricated by LPE.

4.2.1 MBE samples

ศูนย์วิทยทรัพยากร
จุฬาลงกรณ์มหาวิทยาลัย

The sample **A** is Schottky type solar cell grown by MBE. This sample is used as a reference for spectral response and photoluminescence measurements. The spectral response gives basic information about the photon absorption in semiconductor materials used in the heterostructure.

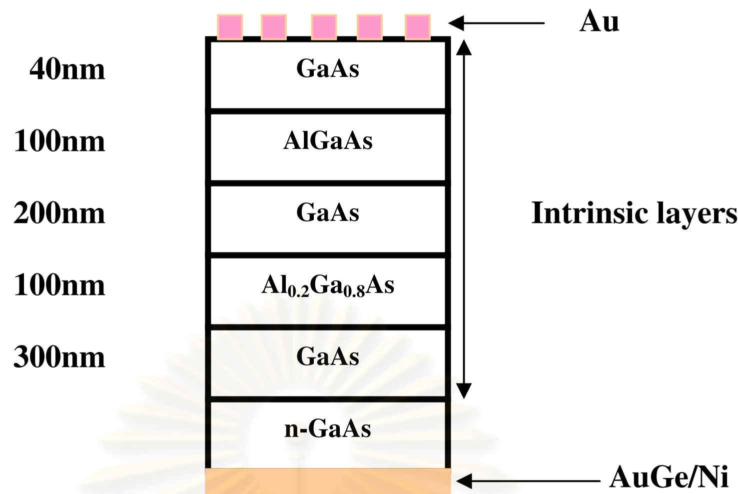

Figure 4.1 Schematic diagrams of Schottky heterostructure solar cells (sample **A**).

The n-GaAs substrate is used as the starting material for solid-source MBE growth of different crystalline layers in Schottky heterostructure solar cells. After desorbing native oxide at 580°C, the temperature is increased up to 610°C for 15 minutes. The substrate temperature is then set back to 580°C. The epitaxial growth of 300nm-thick undoped GaAs buffer layer is conducted at 580°C with a growth rate 0.6 monolayer per second (ML/s). During the growth, the beam equivalent pressure of As_4 was $1x10^{-5}$mbar. The in-situ observation is done by employing the reflection high-energy electron diffraction (RHEED), which has been widely used for the study of the MBE kinetics and can be used to observe the crystal quality during the MBE growth. Then at the same temperature, a 100nm undoped $Al_{0.2}Ga_{0.8}As$, a 200nm undoped GaAs, 100nm undoped AlGaAs and 40nm undoped GaAs are grown respectively. The whole growth process is conducted at growth rate of 0.6 monolayer per second. The sample is taken out from MBE chamber for further metal evaporation. Au was evaporated to form Schottky metallic contact on the front side of solar cells by a finger-shape pattern metallic mask in the vacuum evaporation machine. On the other side of the sample, AuGe/Ni was deposited on over the whole

back surface. To form the Ohmic contact, the sample is annealed in N_2 flowing gas at 375°C. Finally the sample is tested for its spectral response and PL.

In sample **B**, p-GaAs substrate is used as the starting material for solid-source MBE growth of different crystalline layers of heterojunction solar cell with fixed Al content of 0.3. After de-oxidation at 580°C, the temperature is increased up to 610°C for 15 minutes, and then the temperature is set back to 580°C for the whole growth process. The epitaxial growth starts with 500nm-thick undoped GaAs buffer layer. Then a 50nm n-GaAs with doping concentration of $1x10^{18}cm^{-3}$ and a 60nm of $Al_{0.3}Ga_{0.7}As$ layer are grown. Finally, n^+-GaAs with thickness of 50nm and doping concentration of $5x10^{18}cm^{-3}$ are grown. All process is controlled at the same growth rate of 0.7 monolayer per second (ML/s). After the MBE growth, AuGe/Ni is evaporated to form double metallic layers on the front side of the sample through a finger-shape pattern metallic mask in the vacuum evaporation machine. The sample was then annealed in N_2 ambient at 500°C about 2 minutes to obtain the Ohmic contact. Then on the back surface of sample, AuZn is deposited. To achieve the Ohmic contact, the sample is annealed again in N_2 flowing gas at 500°C about 2 minutes.

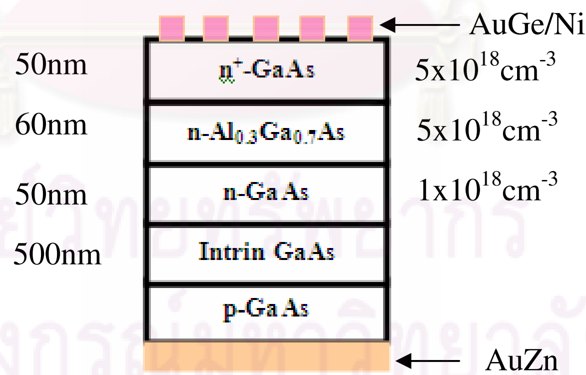

Figure 4.2 Schematic diagram of heterojunction solar cells with fixed Al content of 0.3 (sample **B**).

The preparation of sample **C** is similar to sample **B**. The only change is to replace fixed Al content layer with stepped Al mole fractions in each of AlGaAs

layers. The Al content in each layer is set up at 0.1, 0.2 and 0.3 respectively to increase the band gap of window layer.

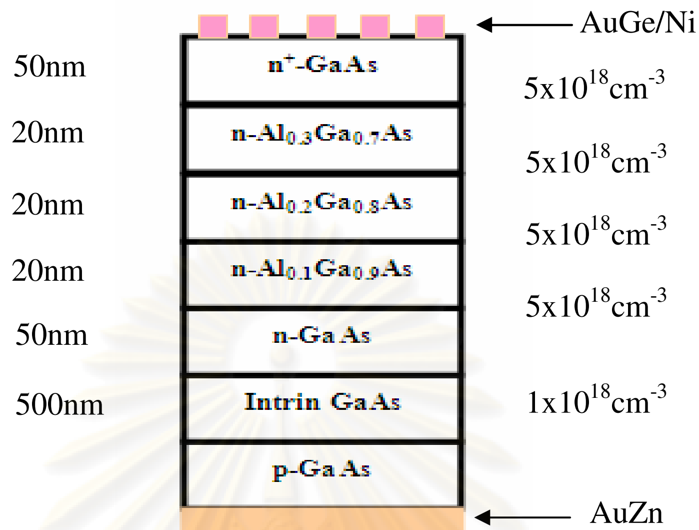

Figure 4.3 Schematic diagram of heterojunction solar cell having $Al_xGa_{1-x}As$ window with stepped Al mole fractions (sample **C**).

The sample **D** has, carrier concentration and layer thickness of n^+-GaAs, $Al_{0.1}Ga_{0.9}As$, $Al_{0.2}Ga_{0.8}As$ and $Al_{0.3}Ga_{0.7}As$ the same as those of sample **C**, but the undoped GaAs buffer layer is 200nm thick.

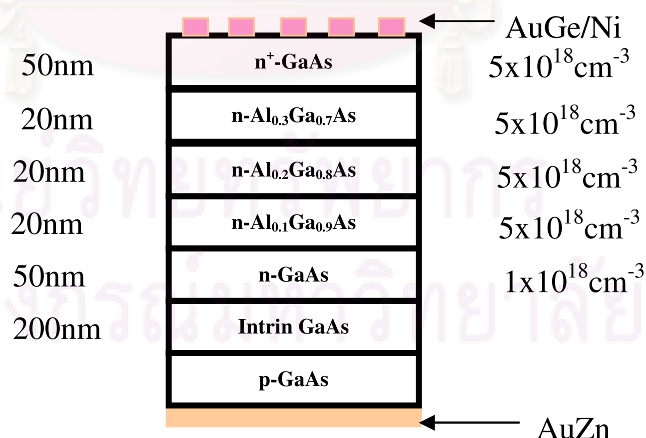

Figure 4.4 Schematic diagram of heterojunction solar cell, the $Al_xGa_{1-x}As$ window with a stepped Al mole fraction having thin 200nm GaAs buffer layer (sample **D**).

The structure of sample **E** is exactly the same as sample **D,** but the carrier concentrations of n-GaAs, $Al_{0.1}Ga_{0.9}As$, $Al_{0.2}Ga_{0.8}As$ and $Al_{0.3}Ga_{0.7}As$ are $1x10^{18}m^{-3}$ as shown in **figure 4.5**.

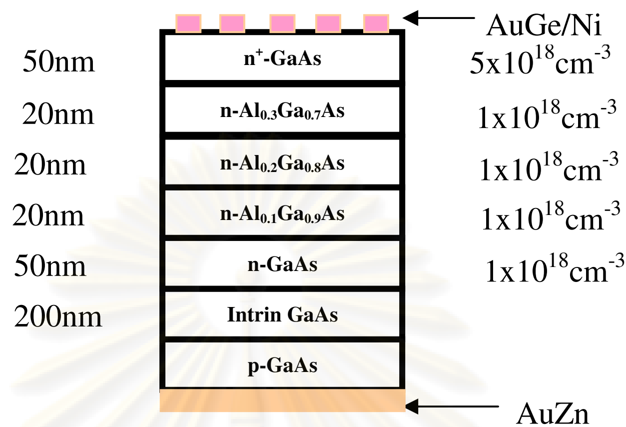

Figure 4.5 Schematic diagram of heterojunction solar cell, the $Al_xGa_{1-x}As$ window with a stepped Al mole fraction (sample **E**).

The last MBE sample **F** has intrinsic layer GaAs and n-GaAs similar to sample **E,** but one more window layer of n-$Al_{0.37}Ga_{0.63}As$ is added to the structure as shown in the **figure 4.6**.

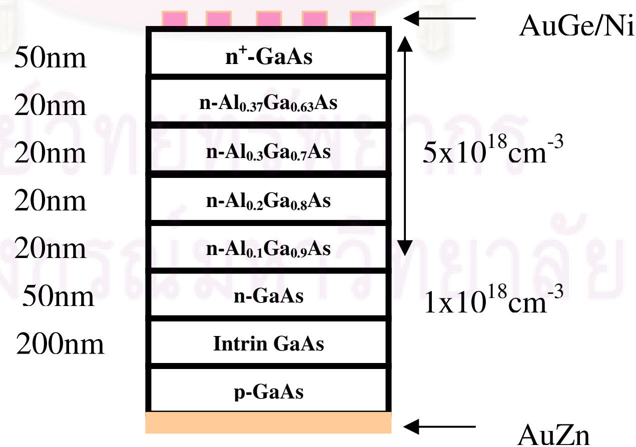

Figure 4.6 Schematic diagram of heterojunction solar cell, the $Al_xGa_{1-x}As$ window with a stepped Al mole fraction (sample **F**).

4.2.2 LPE samples

Two heterostructure solar cells are also fabricated by liquid phase epitaxy (LPE) technique. These LPE samples are compared to pervious MBE samples. It is noticeable that n-GaAs substrate is used as starting material in this LPE technique. The structures of these two LPE samples are shown in **figure 4.7 (a)** and **(b)** respectively.

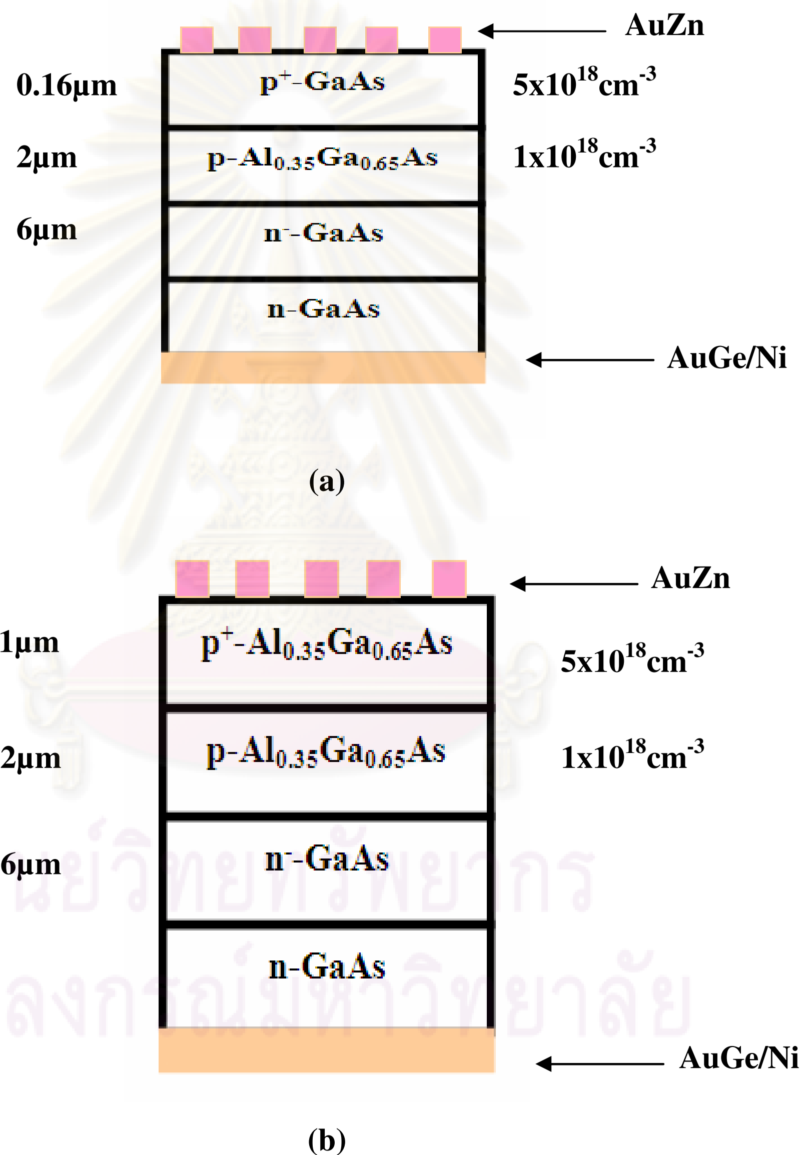

ศูนย์วิทยทรัพยากร
จุฬาลงกรณ์มหาวิทยาลัย

Figure 4.7 (a), (b) Schematic diagram of the heterostructure solar cells, (sample **G** and **H**) grown by LPE technique.

After preparing the materials on the **table 3.1,** graphite boat containing difference materials in multiple slots is loaded into the quartz tube. The boat initially remains outside the heating coil of LPE furnace. First, it is flushed with flowing N_2 in order to evaluate and to check for leaks (approximately 1 hour). Then it is safe to flow with Pd-purified H_2. H_2 atmosphere prevents oxidation of the solution and the substrate. The heating furnace is then slided to the position of the graphite boat. In the first processing step, the temperature is kept constant at 800°C for 4 hours in order to saturate material solutions and then the temperature is increased to 804°C for in-situ etching. When the temperature reaches the peak of 804°C, LPE process starts. For the sample **G,** 6µm thick n-GaAs layer is grown by moving the substrate under the solution consisting of Ga 3g, GaAs 140mg for 6 minutes. Then $Al_{0.35}Ga_{0.65}As$ (p) 2µm thick is grown by moving the substrate under the solution consist of Ga 3g, GaAs 62.1mg, Al 2.89mg and Ge 12.4mg for 2 minutes. Finally, the substrate is moved to the solution consisting of Ga 3g, GaAs 142.2mg and Ge 64.9mg for another 10 second to grow 0.16µm GaAs (p^+) thick. When the sample is moved from solution, the LPE growth is finished. The growth process of sample **H** is the same as that of sample **G**, but GaAs (p^+) layer is replaced by $Al_{0.35}Ga_{0.65}As$ (p^+) as shown in the **figure 4.7 (b)**. LPE samples are metalized with AuZn on the front side through finger-shape pattern metallic mask in the vacuum. The samples are annealed in N_2 ambient at 500°C to obtain the Ohmic contact. On the rear side of the samples, AuGe and Ni are deposited on the whole surface for Ohmic contact. The samples are annealed again in N_2 flowing gas at 500°C. The LPE samples are ready for testing such as their spectral responses and I-V curves.

4.3 Results and discussion

The photoluminescence (PL), the spectral responses and I-V curves characteristics of the samples grown by MBE and LPE are investigated and compared. The experiment results are as follows.

- **Spectral responses**

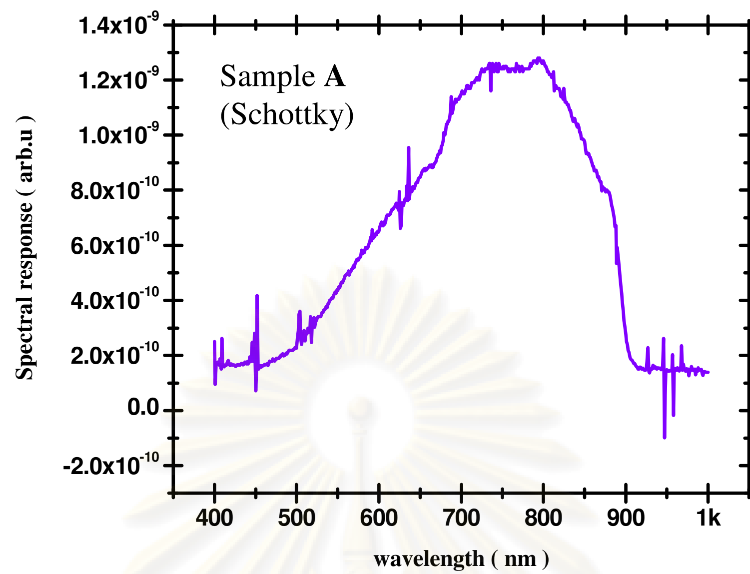

(a)

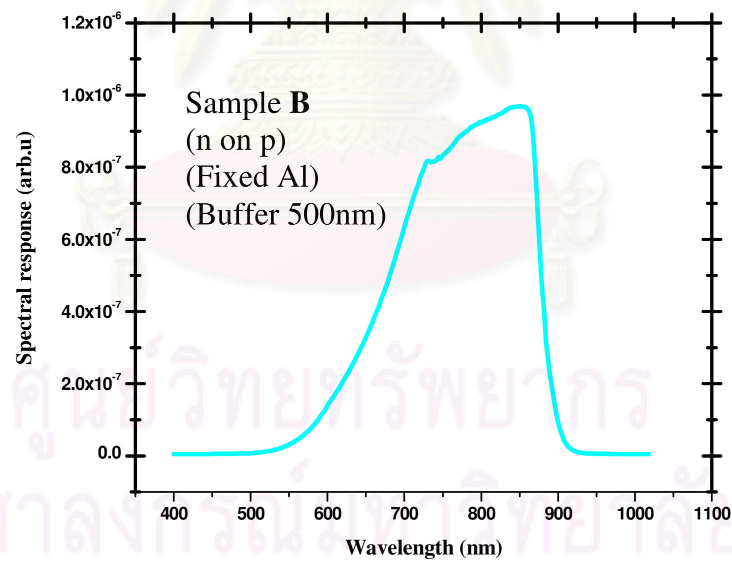

(b)

ศูนย์วิทยทรัพยากร
จุฬาลงกรณ์มหาวิทยาลัย

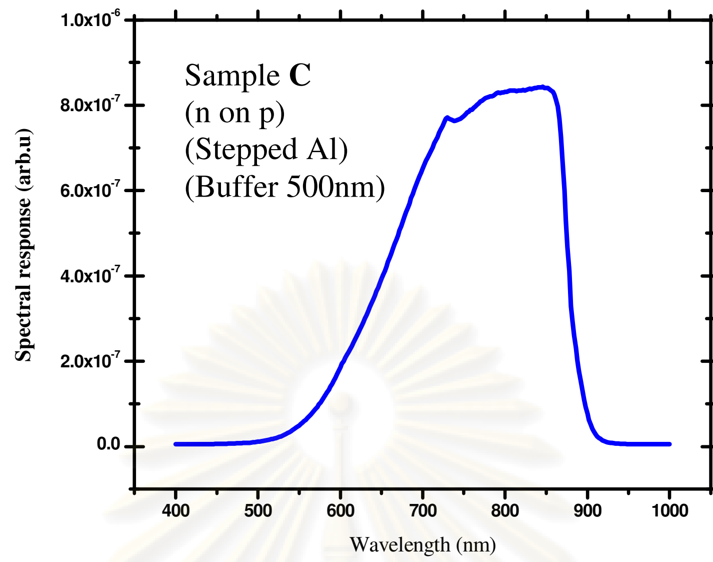

(c)

Figure 4.8 (a), (b) and **(c)** Spectral responses of samples **A, B** and **C**

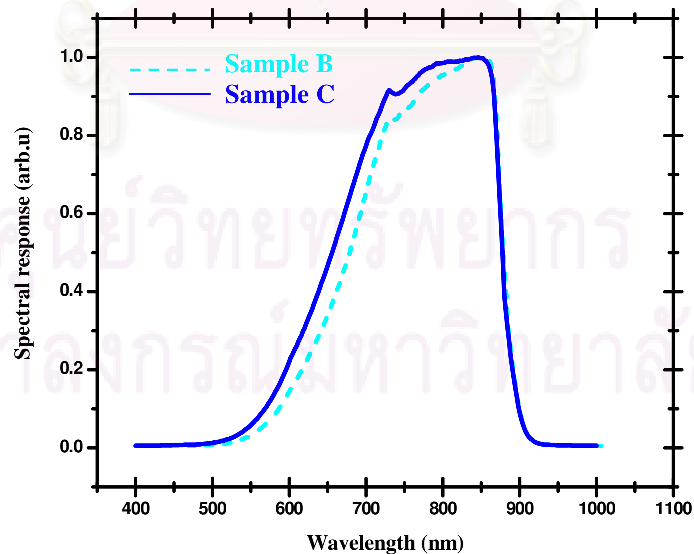

Figure 4.9 Normalized spectral responses of samples **B** and **C**

ศูนย์วิทยทรัพยากร
จุฬาลงกรณ์มหาวิทยาลัย

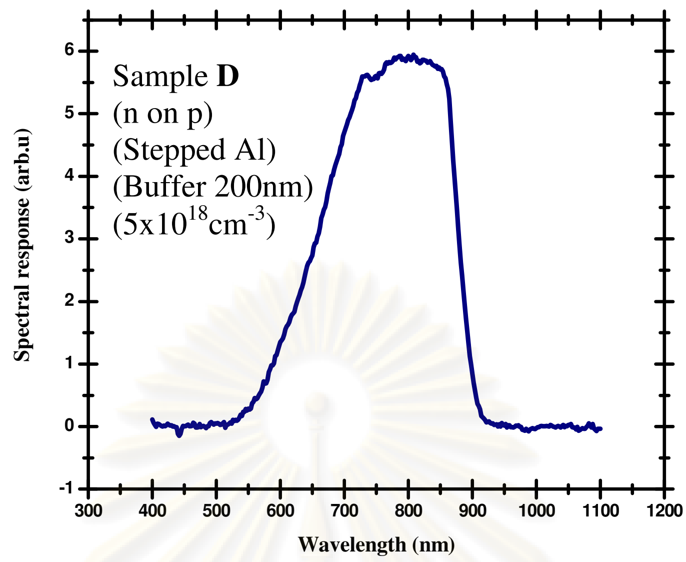

(a)

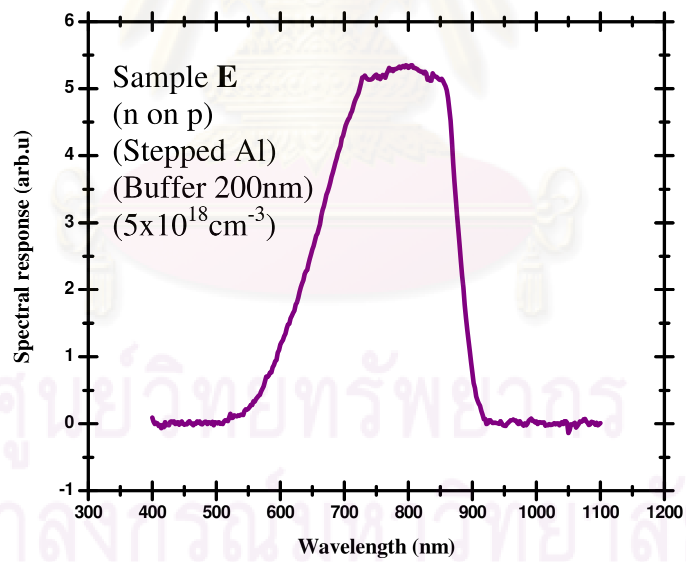

(b)

ศูนย์วิทยทรัพยากร
จุฬาลงกรณ์มหาวิทยาลัย

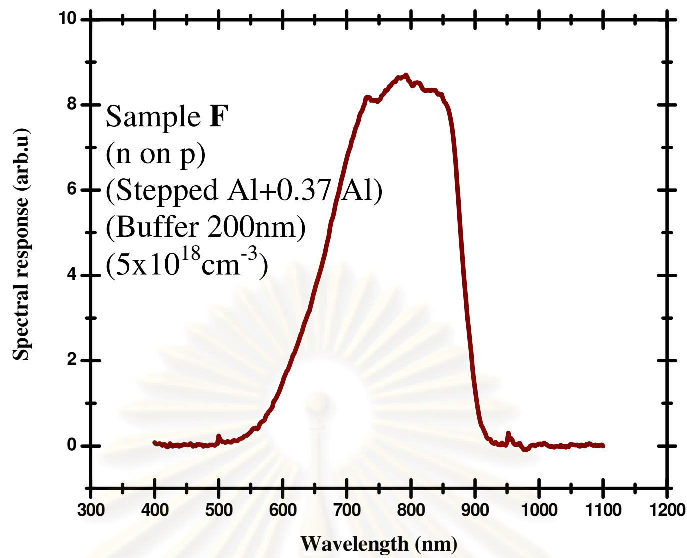

(c)

Figure 4.10 (a), (b) and **(c)** Spectral responses of samples **D, E** and **F**

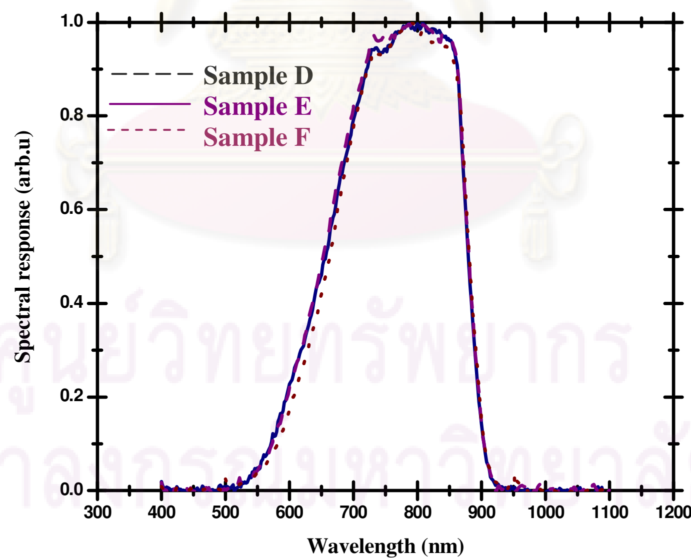

Figure 4.11 Normalized spectral responses of samples **D, E** and **F**

The spectral responses of AlGaAs/GaAs heterostructure solar cells, sample **A**, **B** and **C,** are measured. The board spectrum of photocurrent ranging from 700 to 900

nm could be explained by the window effect of AlGaAs having a wide direct band gap especially at the short wavelength region. The spectral responses of samples **B**, **C** are also measured for comparison as shown in the **Figure 4.9**. It is found that the spectral response of sample **C** is better than those of samples **B.**

The spectral responses of the sample **D, E** and **F** are similar to each other as shown in the **Figure 4.11**

In general, wide band gap AlGaAs layers are preferable in the solar cell structure.

- **Photoluminescence (PL)**

The photoluminescence measurement of samples **A, B** and **C** were conducted at temperature 20°K by using Ar^+ laser with excitation power of 20mW. Sharp PL peaks of sample **A, B** and **C** are at 812, 842 and 842nm respectively. These PL peaks are evident that epitaxial layers have good crystalline quality for device fabrication.

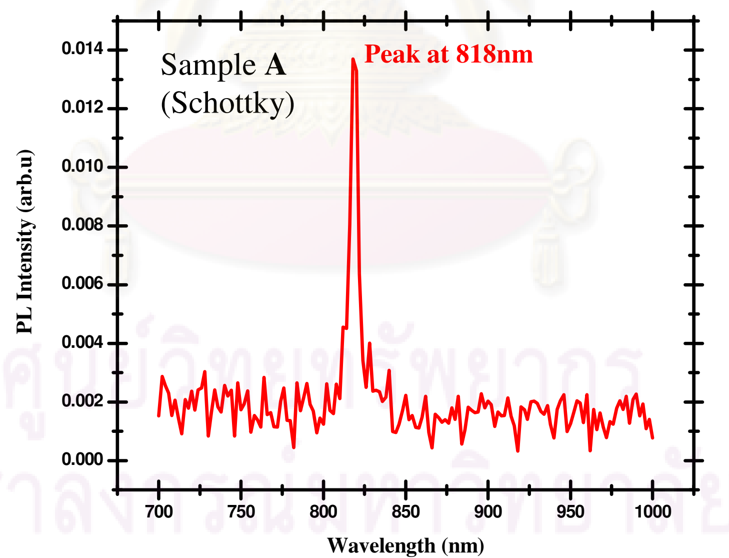

(a)

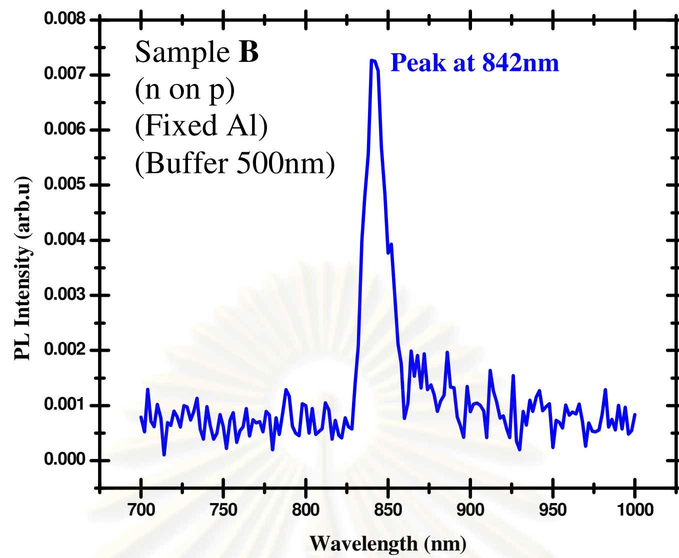

(b)

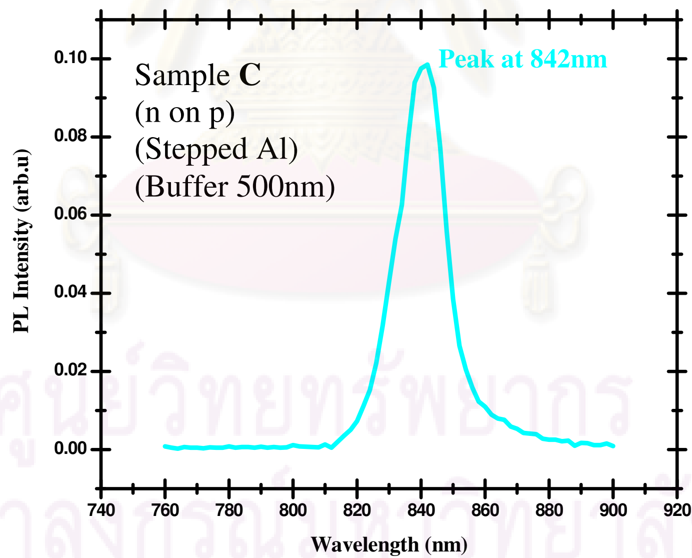

(c)

Figure 4.12 (a), (b) and **(c)** Photoluminescence of samples **A, B** and **C,** respectively

ศูนย์วิทยทรัพยากร
จุฬาลงกรณ์มหาวิทยาลัย

- **The I-V curve characteristics**

All MBE samples having AlGaAs/GaAs heterostructures are tested for their respective I-V curves both under dark and illuminated condition of one sun (100mW/cm^2 and AM1). The I-V curves are displayed in the following figures.

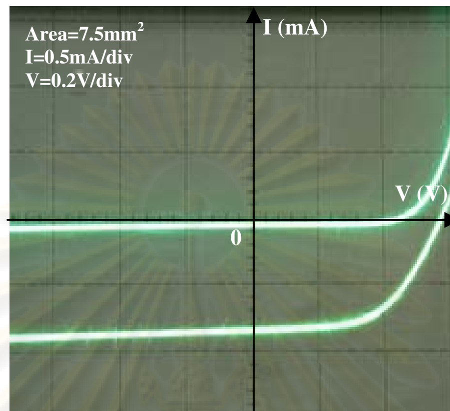

Sample **B**
(n on p)
(Fixed Al)
(Buffer 500nm)

I_{SC}=0.85mA
V_{OC}=0.59V
I_{max}=0.7mA
V_{max}=0.42V

(a)

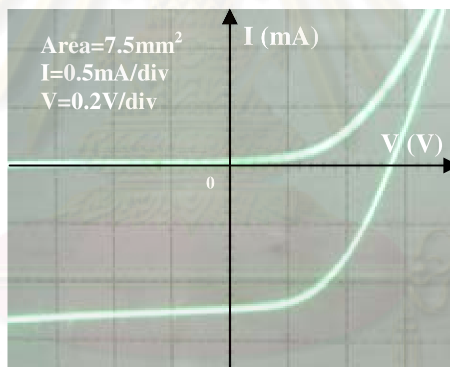

Sample **C**
(n on p)
(Stepped Al)
(Buffer 500nm)

I_{SC}=1.25mA
V_{OC}=0.58V
I_{max}=0.7mA
V_{max}=0.4V

(b)

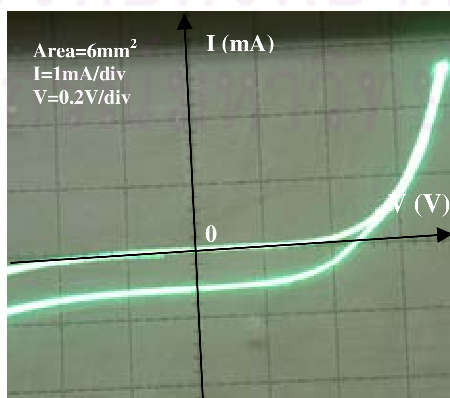

Sample **D**
(n on p)
(Stepped Al)
(Buffer 200nm)
(5x10^{18}cm^{-3})

I_{SC}=0.6mA
V_{OC}=0.5V
I_{max}=0.4mA
V_{max}=0.38V

(c)

ศูนย์วิทยทรัพยากร
จุฬาลงกรณ์มหาวิทยาลัย

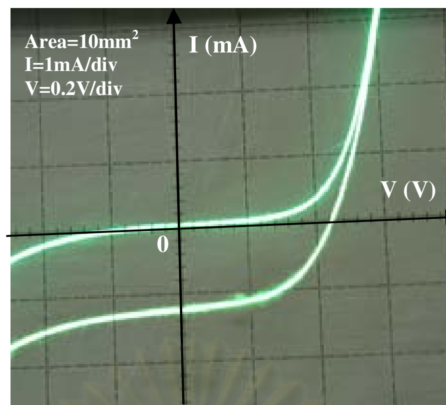

Sample **E**
(n on p)
(Stepped Al)
(Buffer 200nm)
($5x10^{18}cm^{-3}$)

I_{SC}=1.3mA
V_{OC}=0.43V
I_{max}=0.9mA
V_{max}=0.38V

(d)

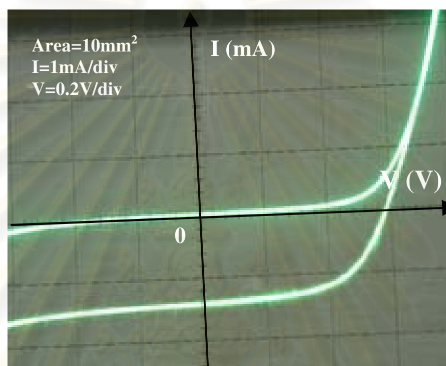

Sample **F**
(n on p)
(Stepped Al+0.37 Al)
(Buffer 200nm)
($5x10^{18}cm^{-3}$)

I_{SC}=1.5mA
V_{OC}=0.6V
I_{max}=1mA
V_{max}=0.5V

(e)

Figure 4.13 (a), (b), (c), (d) and **(e)** I-V curves in dark and one sun of AlGaAs/GaAs heterostructure solar cells, samples **B**, **C, D, E** and **F** respectively.

From these I-V curves, all solar cell parameters are summarized in **table 4.1.** It is found that most of MBE samples give rather low open circuit voltages not greater than 0.6V. The breakdown voltage is quite low as observed in the third quadrant of I-V curves. This implies that junction quality is not good. There are some leakage current in the junction. The best efficiency from this group of MBE samples is only 5%. This solar performance could be improved by high doping of p^+ at the back surface of p-GaAs substrate.

Table 4.1 Solar cell parameters of samples **B, C, D, E** and **F**

Sample	Area(mm^2)	I_{Sc}(mA)	V_{Oc}(V)	I_{max}(mA)	V_{max}(V)	FF	η (%)
B	7.5	0.85	0.59	0.7	0.42	0.58	3.86
C	5.5	1.25	0.58	0.7	0.4	0.38	5
D	6	0.6	0.5	0.4	0.38	0.47	2.3
E	10	1.3	0.43	0.9	0.38	0.61	3.4
F	10	1.5	0.6	1	0.5	0.55	4.9

- **Spectral responses**

The spectral responses of both samples **G** and **H** are also measured and exhibit a strong absorption edge by n-GaAs substrate 900nm as shown in **figure 4.14.**

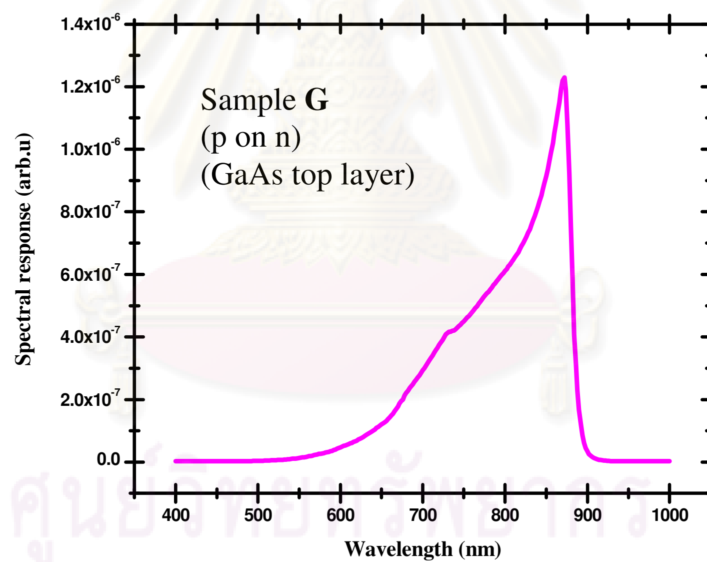

(a)

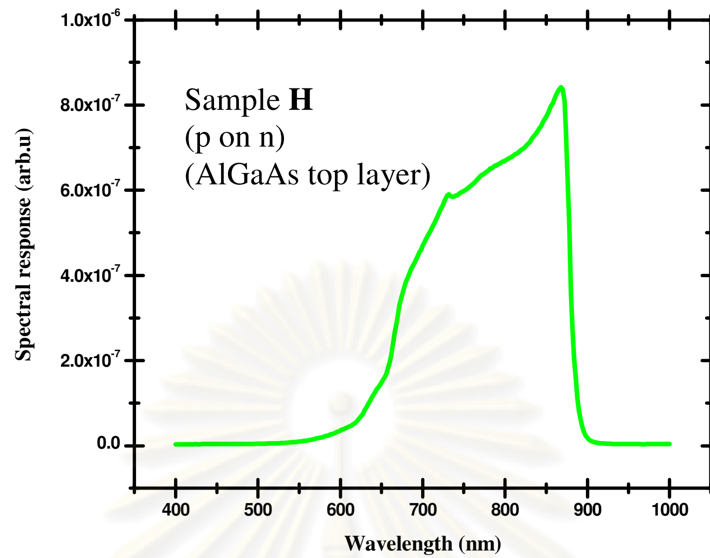

(b)

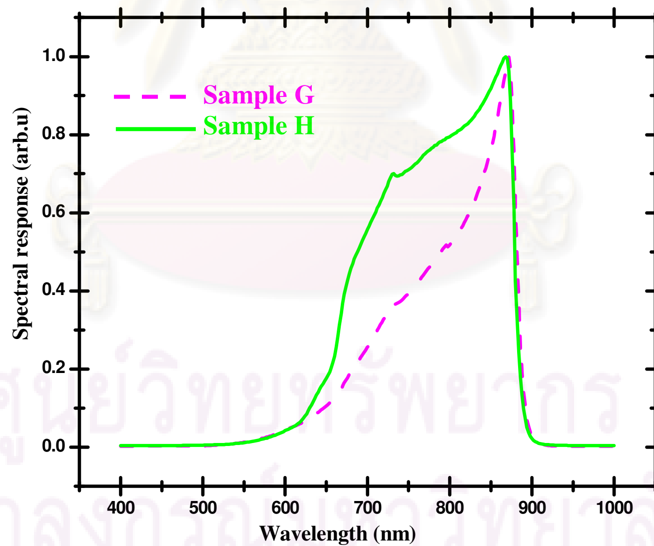

(c)

Figure 4.14 (a) Spectral responses of sample **G**, **(b)** Spectral responses of sample **H** and **(c)** normalized spectral responses of sample **G** and **H**

- **The I-V curve characteristics**

The LPE samples are tested for their I-V curves at dark and one sun illumination (100mW/cm^2 and AM1). The experimental results are displayed in **figure 4.15 (a)** and **(b)** respectively. All solar cell parameters are summarized in **table 4.2.** It is observed that the breakdown voltage is improved. V_{OC} of sample **I** is 0.7V which is higher than those of MBE samples. However, over all I-V curves characteristics are not improved. The efficiency of LPE samples is comparable with those of MBE samples.

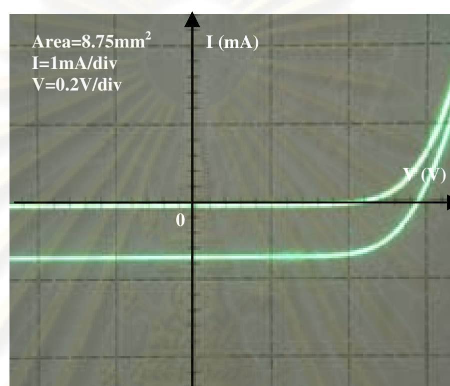

Sample **G**
(p on n)
(GaAs top layer)

I_{Sc}=0.8mA
V_{Oc}=0.59V
I_{max}=0.6mA
V_{max}=0.58V

(a)

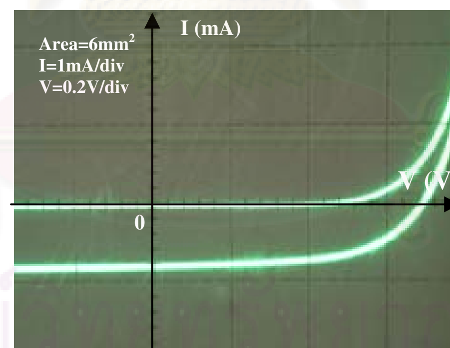

Sample **H**
(p on n)
(AlGaAs top layer)

I_{Sc}=0.9mA
V_{Oc}=0.7V
I_{max}=0.6mA
V_{max}=0.48V

(b)

Figure 4.15 (a) and **(b)** I-V curves in the dark and one sun of AlGaAs/GaAs heterostructure solar cells, sample **G** and **H** respectively**.**

ศูนย์วิทยทรัพยากร
จุฬาลงกรณ์มหาวิทยาลัย

Table 4.2 The calculated solar cell's output parameters of sample **G** and **H**

Sample	Area(mm^2)	I_{Sc}(mA)	V_{Oc}(V)	I_{max}(mA	V_{max}(V)	FF	η (%)
G	8.75	0.8	0.59	0.6	0.48	0.61	3.2
H	6	0.9	0.7	0.6	0.48	0.45	4.7

All MBE samples are grown on p-type GaAs substrate. The epitaxial layers are undoped GaAs, n-GaAs, and $Al_xGa_{1-x}As$ window layer. Finally, very thin layer of n^+-GaAs for Ohmic contact is grown on the top-most surface. All MBE sample structures are illustrated in **figure 4.2, 4.3, 4.4, 4.5** and **4.6** respectively. All MBE samples are tested for their spectral responses, I-V curve characteristics. Solar cell parameters such as voltage, current, fill factor and efficiency are calculated from I-V curves. It is observable from **table 4.1** that both V_{OC} and I_{SC} are too low. These can be explained that the heterojunction is not in good quality. There are some junction leakages leading to low V_{OC}. The high series resistance due to too low doping density and contact resistance give small I_{SC}. Therefore, the efficiencies of those MBE grown solar cells are low. One technical problem is that we do not have p-type dopant source in our MBE system. Hence, p^+ doping for back surface field is not possible in our experiment.

LPE samples (samples **G** and **H**) are grown on n-type GaAs substrate. The epitaxial growth is conducted from undoped GaAs, p-GaAs, to p-$Al_{0.35}Ga_{0.65}As$ window layer, respectively. Very thin layer of p^+-GaAs is used for Ohmic contact. All LPE samples are tested for their spectral responses and I-V curve characteristics. It is found from our experiment data that LPE samples have some improvement in their V_{OC} due to better junction quality. However, too thick epitaxial layers grown by LPE lead to large junction depth. The absorbed photons are not effectively in producing high I_{SC}. Therefore, our LPE samples are not good solar cells due to the uncontrollability of epitaxial layer thickness below 1μm**.**

The comparison between MBE and LPE growth techniques for heterostructure solar cells can give some technical information as follows. MBE can provide very thin epitaxial layers which are ideal for shallow junction devices like solar cells. However, junction properties and doping profiles should be carefully designed to provide both

high value of V_{OC} and I_{SC} as well as the fill factor. LPE growth technique is appropriate for thick epitaxial layers having good crystal quality for most of electronic devices, but LPE can not provide shallow junction depth for solar cell application.

ศูนย์วิทยทรัพยากร
จุฬาลงกรณ์มหาวิทยาลัย

CHAPTER V
CONCLUSIONS

5.1 Heterostructure solar cells

Fabrication of AlGaAs/GaAs heterostructure solar cells has been conducted in this research by using both MBE and LPE growth techniques. There are six MBE samples having different detailed structures. These solar cell performances are compared to other two LPE samples. All MBE and LPE samples are tested for their spectral responses and I-V curve characteristics. All solar cell parameters are measured and calculated. It is being confirmed that wide gap AlGaAs window layers give better spectral response at short wavelength region. I-V curves at dark indicate the junction quality, e.g. leakage current and breakdown voltage. I-V curves at one sun illumination give information of solar cell parameters and efficiency.

In our experiment results, the efficiency of AlGaAs/GaAs solar cell is only 5% which is too small from the best data of more than 20%. This discrepancy comes from improper design of the devices as well as lack of experience in solar fabrication of the author.

5.2 Limitation of study

There is some time constraint in this research project which was conducted in few months time. However, in our discussion, we have mentioned some technical points which can be improved for better efficiency of the solar cells.

5.3 Further study

It is suggested that further study should be conducted on this research topic by additional experimental procedures.

1) Each sample should be coated by anti-reflection layer on the top of solar cell.
2) And each sample should be heavily doped on the rear surface for back surface field.

REFERENCES

[1] Richard C. Neville. Solar Energy Conversion, the Solar cell, Second Edition, College of Engineering & Technology Northern Arizona University Flagstaff, AZ, U.S.A.

[2] London• Sterling, VA. Planning and Installing Photovoltaic Systems, a Guide for Installers, Architects and Engineers, Second Edition.

[3] Tom Markvart & Luis Castañer. Practical Handbook of Photovoltaic, Fundamental and Applications.

[4] Chapin D, Fuller C, Pearson G, J. Appl. Phys. (1954).

[5] Reynolds D, Leies G, Antes L, Marburger R. Phys. Rev. (1954).

[6] Jenny D, Loferski J, Rappaport P. Phys. Rev. (1956).

[7] Antonio Luque, Instituto de Energía Solar. Handbook of Photovoltaic Science and Engineering.Universidad Politécnica de Madrid, Spain, Steven Hegedus, Institute of Energy Conversion, University of Delaware, USA.

[8] Z.I. Alferov, V.M. Andreev, and V.D. Rumyantsev. III–V Solar Cells and Concentrator Arrays.

[9] J. P. Colinge**.** Physic of Semiconductor Devices. Department of Electrical and Computer Engineering University of California, Davis, C. A. Colinge**,** Department of Electrical and Electronic Engineering California State University.

[10] Jenny Nelson, Imperial College, UK. The Physics of Solar cells.

[11] H.J. Hovel. Semiconductors and Semimetals. Academic Press (1975).

[12] B.L. Sharma, R.K. Purohit. Semiconductor Heterojunctions, Pergamon Press (1974).

[13] H. Nelson. Epitaxial grwth from the liquid state and its application to fabrication of tunnel and laser diode. RCA (1963).

[14] M.B Panish, I. Hayashi, S. Sumski. Double-heterostructure injection lasers with room temperature thresholds as low as 2300A/cm^2. Appl. Phys (1970).

[15] Zh. Alferov, V.M. Andreev, D.Z. Garbuzov, Yu. V. Zhilyaev, E.P. Morozov, E.L. Portnoi, V.G. Trofim. Investigation of the influence of AlAs-GaAs

heterostructure parameters on the laser threshold current and the realization of the continuous emission at the room temperature. Sov. Phys. Semicond (1971).

[16] J.J. Harris, B.A. Joyce, P.J. Dobson, Oscillations in the surface structure of Sn-doped GaAs during growth by MBE. Surf. Sci. (1981).

[17] W. Braun. Applied RHEED-Reflection High Energy Electron Diffraction during Crystal Growth, Springer Tracts in Modern Physics. Springer, Berlin, 1999.

[18] Herman, M. A., and Sitter, H. 1989. Molecular Beam Epitaxy Fundamental and Current Status. Springer-Verlag, Berlin.

[19] Hummel, S. G., Zou, Y., Beyler, C. A., Grodzinski, P., and Dapkus P. D., McManus J. V., Zhang. Y., and Skromme, B. J. 1992. Characteristics of GaAs, AlGaAs, and InGaAs materials grown by metalorganic chemical vapor deposition using an on-demand hydride gas generator. Applied Physics.

[20] G.D. Gilliland. Photoluminescence spectroscopy of crystalline semiconductors. Emory Umversity, Phys Department, Atlanta, GA 30322, USA.

[21] Pakawat Wisetlakhorn. Fabrication and study on spectral response of GaAs/AlGaAs staircase band gap photodiode. Chulalongkorn University, Faculty of Engineering (2003).

ศูนย์วิทยทรัพยากร
จุฬาลงกรณ์มหาวิทยาลัย

BIOGRAPHY

Bounpone Keomanivong was born on May 1, 1983 in Champasak province, the south of Laos, he spent his time for academic study from primary school until finishing high school in Champasak. He succeeded in obtaining a Bachelor Degree from National University of Laos, Faculty of Engineering and Electronic Department in 2007. He was promptly awarded AUN/SEED-Net JICA scholarship which formally admitted him to pursue his Master Degree in a field of Electrical Engineering, Chulalongkorn University, Thailand.

ศูนย์วิทยทรัพยากร
จุฬาลงกรณ์มหาวิทยาลัย